

Highlights

Estimation of aboveground biomass in a tropical dry forest: An intercomparison of airborne, unmanned, and space laser scanning

Nelson Mattié, Arturo Sanchez-Azofeifa, Pablo Crespo-Peremarch, Juan-Ygnacio López-Hernández

- **Critical Context:** This study addresses the urgent need for high-quality forest data, as required by the Paris Agreement, by focusing on tropical dry forests, one of the least understood tropical ecosystems.
- **Innovative Methodological Approach:** A comparative analysis of laser scanning methods (discrete and full-waveform airborne, drone, and spaceborne) is combined with a machine learning approach (Support Vector Machines, SVM) to estimate aboveground biomass (AGB).
- **Key Variables Identified:** Metrics related to tree height were found to be crucial for discrete laser systems (ALS and ULS), while Leaf Area Index, canopy cover, and full-waveform signal energy were most vital for the spaceborne system (SLS).
- **High Accuracy Achieved:** The SVM regression model achieved a notably low error 17.89% in estimating AGB, with spaceborne full-waveform lidar (SLS_FW) being the most accurate 17.07%*error*.
- **Policy Relevance:** The research demonstrates how laser scanning technology can significantly improve forest carbon estimates, providing a vital tool for nations to meet their reporting obligations under the Paris Agreement.

Estimation of aboveground biomass in a tropical dry forest: An intercomparison of airborne, unmanned, and space laser scanning

Nelson Mattié^a, Arturo Sanchez-Azofeifa^a, Pablo Crespo-Peremarch^b and Juan-Ygnacio López-Hernández^c

^aUniversity of Alberta, Alberta Centre for Earth Observation Sciences, Department of Earth and Atmospheric Sciences, University of Alberta, AB, T6G 2E3, Edmonton, Canada

^a*Correspondence

^bUniversitat Politècnica de València, Geo-Environmental Cartography and Remote Sensing Group (CGAT), Department of Cartographic Engineering, Geodesy and Photogrammetry, Camí de Vera s/n, 46022, València, Spain

^cUniversity of Los Andes, Photogrammetry and Remote Sensing Laboratory, Vía Chorros de Milla, 1511, Mérida, Venezuela

ARTICLE INFO

Keywords:

Tropical dry forest
carbon cycle
carbon stock
GHG
forest inventory
forest monitoring
remote sensing

ABSTRACT

According to the Paris Climate Change Agreement, all participating nations are required to submit reports on their greenhouse gas emissions and absorption every two years by 2024. Consequently, forests play a crucial role in reducing carbon emissions, which is essential for meeting these obligations. Recognizing the significance of forest conservation in the global battle against climate change, Article 5 of the Paris Agreement emphasizes the need for high-quality forest data. This study focuses on enhancing methods for mapping aboveground biomass (AGB) in tropical dry forests. Tropical dry forests are considered one of the least understood tropical forest environments; therefore, there is a need for accurate approaches to estimate carbon pools. We employ a comparative analysis of AGB estimates, utilizing different discrete (D) and full-waveform (FW) laser scanning datasets in conjunction with Ordinary Least Squares (OLS) and Bayesian approaches (Support Vector Machines, SVM). Airborne Laser Scanning (ALS_D), Unmanned Laser Scanning (ULS_D), and Space Laser Scanning (SLS_{FW}) were used as independent variables for extracting forest metrics. Variable selection, SVM regression tuning, and cross-validation via a machine-learning approach were applied to account for overfitting and underfitting. The results indicate that six key variables primarily related to tree height (Elev.minimum, Elev.L3, Elev.MAD.mode, Elev.mode, Elev.MAD.median, and Elev.skewness) are important for AGB estimation using ALS_D and ULS_D , while Leaf Area Index, canopy coverage and height, terrain elevation, and full-waveform signal energy emerged as the most vital variables for SLS_{FW} . AGB values estimated from ten permanent tropical dry forest plots in Costa Rica's Guanacaste province ranged from $26.02 \text{ Mg}\cdot\text{ha}^{-1}$ to $175.43 \text{ Mg}\cdot\text{ha}^{-1}$. The SVM regressions demonstrated a 17.89% error across all laser scanning systems, with SLS_{FW} exhibiting the lowest error (17.07%) in estimating total biomass per plot. This study highlights how laser scanning data can significantly improve estimates of aboveground forest biomass, which is crucial for meeting the reporting obligations outlined in the Paris Agreement.

1. Introduction

AGB is one of the most important Earth carbon cycle variables, and its accurate estimation is crucial for modeling ecosystem dynamics, supporting conservation policies, and mitigating climate change (Houghton et al., 2009). Remote sensing is an effective method for estimating AGB and quantifying carbon reservoirs. Various studies have estimated AGB using different remote sensing data sources, including synthetic aperture radar (SAR) in the X-, C-, L-, and P-bands, and HH, VV, HV, and VH polarizations (Berninger et al., 2018; Mette et al., 2003; Santos et al., 2004; Schepaschenko et al., 2019), hyperspectral and multispectral optical sensors (de Almeida et al., 2019; Koch, 2010; Narine et al., 2019; Sun et al., 2019), and laser scanning (Ferraz et al., 2018; Hu et al., 2020; Kellner et al., 2019; Luo et al., 2017; Tadese and Soromessa, 2019; Torre-Tojal et al., 2019).

*Corresponding author

 mattiedj@ualberta.ca (N. Mattié)

 gasanche@ualberta.ca (A. Sanchez-Azofeifa); pabcrepe@cfg.upv.es (P. Crespo-Peremarch); jlopez@ula.ve (J. López-Hernández)

ORCID(s): 0000-0003-4882-9865 (N. Mattié); 0000-0001-7768-6600 (A. Sanchez-Azofeifa); 0000-0003-2241-4493 (P. Crespo-Peremarch); 0000-0003-2556-9896 (J. López-Hernández)

For more than 50 years, the National Aeronautics and Space Administration (NASA) and other international space agencies have supported the development of solutions using Earth Observation Systems to estimate forest extent, deforestation, and secondary growth rates, and to document the carbon and water cycles (Kellner et al., 2019). Meanwhile, aboveground biomass (AGB) continues to represent one of the most significant gaps in Earth observation efforts (Dubayah et al., 2020). To fill this gap, NASA launched the Global Ecosystem Dynamics Investigation (GEDI) mission in 2018. GEDI, operating on board the International Space Station from December 2018 to March 2023, was engineered to survey approximately 4% of Earth's land surface during its scheduled two-year operation. The instrument was projected to obtain over 10 billion cloud-free observations of the planet's surface, yielding precise data on forest composition and canopy elevation (Dubayah et al., 2020). Upon fulfilling its primary mission, the GEDI entered a standby phase. In April 2024, the device was reactivated, and the GEDI research team anticipated continued data collection until 2030. Laser scanning observations of the GEDI were used to create datasets for canopy height and coverage, vertical profile, leaf and profile area indices, and AGB. These were the first space measurements of an instrument specifically designed and optimized to measure the structure of vegetation and form the basis of critical reference datasets for the scientific community (Dubayah et al., 2020). Laser scanning has been used to characterize complex forest structures (Koch, 2010). Zolkos et al. (2013) evaluated over 70 studies that estimated AGB and concluded that AGB models derived from laser scanning (i) are significantly more accurate than models that use radar or passive optical sensor data; (ii) combined laser scanning, radar, and passive optical sensors generate greater variability than laser scanning alone, and they do not always improve biomass estimates; (iii) a model's accuracy varies depending on the type of forest; and (iv) concerning the magnitude of the field biomass, model errors decreased as the size and number of plots increased.

Laser-scanning data can vary based on different characteristics, such as the platform on which the sensors are installed or the format in which the data are recorded. In terms of the platform, along with Terrestrial Laser Scanning or Mobile Laser Scanning, we have Airborne Laser Scanning (ALS_D), Unmanned Laser Scanning (ULS_D), and Space Laser Scanning (SLS_{FW}) platforms. Owing to their cost-efficiency, coverage, and scalability, ALS and ULS are the most suitable options for mapping biomass at the local or regional scale. In contrast, SLS allows the mapping of biomass both nationally and globally (Luo et al., 2019). Likewise, laser-scanning data can be separated into discrete- and full-waveform data according to the format of the recorded information. Discrete data record the elements whose intensity value is the highest in the shape of a cloud of 3D points (such as treetops, branches, trunks, and ground). In contrast, full-waveform data record the entire waveform of the laser pulse that passes through the different vertical layers of the forest (Crespo-Peremarch, 2020). Discrete laser scanning has proven to be appropriate for most current applications. Nevertheless, full-waveform laser scanning can characterize the intermediate and lower layers of vegetation in a precise and detailed manner (Crespo-Peremarch, 2020). Despite this precision and detailed characteristics, there is still debate surrounding the type of laser scanning and the most appropriate data format for estimating AGB in tropical forests (Sanchez-Azofeifa et al., 2017).

To achieve model parsimony in explaining the AGB, we strive to employ the fewest possible variables, tackling the challenge of laser-scanning discrete point clouds potentially generating an excess of variables. This parsimonious approach was previously applied to GEDI data by Duncanson et al. (2022). In addition, Generalized Additive Models (GAMs) are employed to classify model variables by their significance in biomass prediction, a method previously utilized in a model by Lee et al. (2023) and Nandlall and Millard (2020). Once the candidate variables for the model are selected, the hyperparameters for the SVM regression are explored (Belete and Manjaiah, 2021). SVM regression can be employed with various kernel options, including linear, polynomial, radial basis function (RBF), and sigmoid (Yang and Shami, 2020). The hyperparameters can be determined, and the final set of variables for the regression model can be defined using the leave-one-out cross-validation method (Kudo et al., 2023). After fitting the regression model, it is crucial to analyze the errors to prevent underfitting or overfitting (Ramasubramanian and Singh, 2019). The evolution of errors in each iteration of the regression can be assessed to verify the absence of overfitting and gauge the overall quality of the final model.

Owing to the variability in scanning patterns, such as scanning angle, flight height, ray divergence, and footprint size, it is extremely challenging to determine the effects of these parameters on the estimation of AGB in tropical forests (Gonçalves, 2014; Silva et al., 2018). In this study, we assessed how ALS_D , ULS_D , and SLS_{FW} laser scanning can be used to estimate AGB in semi-deciduous tropical dry forests using the following approaches: (i) ULS_D with non-repetitive scanning patterns; (ii) ALS_D with linear, repetitive scanning patterns; and (iii) SLS_{FW} simulated from ALS_D data. We evaluate the effectiveness of this approach via (1) the development and test of regression models using

Ordinary Least Squares (OLS) and Support Vector Machines (SVM), and (2) analyzing the error of the regression methods' estimates.

2. Materials and methods

2.1. Study site

The site is located at the Santa Rosa National Park Environmental Monitoring Super Site (SRNP-EMSS) in Guanacaste, Costa Rica. SRNP-EMSS is extensively used to study the linkages between remote sensing at different spatial and spectral scales and the ecology and biodiversity of tropical secondary dry forests (Cao et al., 2015; Zhao et al., 2021). The site has ten permanent plots, monitored annually by the Earth and Atmospheric Sciences Department, Alberta Centre for Earth Observation Sciences (CEOS) of the University of Alberta, Canada, since 1998 (Duan et al., 2023; Liu et al., 2023).

The SRNP-EMSS is a mosaic of semi-deciduous tropical dry forests (fig. 1) in various stages of ecological succession (fig. 2) that suffered heavy deforestation during the 18th, 19th, and 20th centuries (Li et al., 2017). Depending on the age since abandoned ($t_0 = 1971$, when the SRNP was created), forest cover is classified as early (E), intermediate (I), and late (L) (Arroyo-Mora et al., 2005). Early forests in the SRNP-EMSS comprise patches of woody vegetation that include different species of shrubs, small trees, and saplings, with a maximum height of approximately 6–8 m. Trees in the early stages lose almost all their leaves during the dry season. They are dominated by species that are well adapted to open habitats, such as *Cochlospermum vitifolium*, *Gliricidia sepium*, and *Rehdera trinervis*, as well as species that are adapted to the sun, such as heliophytes (Hilje et al., 2015). The intermediate and late successional stages exhibit significant differences in forest structure and composition (Kalacska et al., 2004). These differences are generally due to species turnover (Sun et al., 2019). The intermediate- and late-successional stages typically have two layers of vegetation. The first layer comprises deciduous trees with rapid growth that reach a maximum height of 10–15 m. The second layer is below the canopy and is composed of lianas (woody vines) and adult evergreen trees that are more tolerant to shade and saplings of many species (Hilje et al., 2015; Kalacska et al., 2004). The dominant species in the intermediate stage are *Rehdera trinervis* and *Guazuma ulmifolia*, whereas *Calycophyllum candidissimum* and *Hymenaea courbaril* are dominant in the late stage (Kalacska et al., 2004). Not all trees in the intermediate and late stages are deciduous. There are also various evergreen species, but the proportion of evergreen species does not exceed 20% (Kalacska et al., 2004).

2.1.1. Forest inventory of permanent plots

In 1998, nine permanent plots measuring 0.1 hectares (20 m × 50 m) were established and distributed by successional stage: early (E), intermediate (I), and late (L) (Kalacska et al. (2004)). In addition, a 1 ha plot in an intermediate stage was established in 2010. The plots were set up following Tropi-Dry protocols described by Nassar et al. (2008). All trees with a diameter at breast height (DBH = 1.3 m) greater than 0.05 m are measured annually (1998 until today) to estimate the increase in tree diameter, height, crown diameter, growth, and mortality (Calvo-Rodriguez et al., 2021). Field data at the SRNP-EMSS were collected every rainy season between July and October; the 2021 forest inventory was used in this study because it coincided with the airborne LiDAR data collected in June 2021.

AGB was estimated for each tropical tree species using eq. (1) from Calvo-Rodriguez et al. (2021):

$$AGB = 0.0673 \times (\rho \times DBH^2 \times H)^{0.976} \quad (1)$$

Where AGB is the aboveground biomass, ρ is the wood density (g·cm⁻³), DBH is the diameter at breast height (cm), and H is the tree height (m). Specific wood density values for the species in the SRNP-EMSS were obtained using published and unpublished data (Powers and Tiffin, 2010). When data from the site were unavailable, species or genera from other locations were used (Chave et al., 2009). The forest metrics for the ten permanent plots and their biomass estimates from the 2021 forest inventory are presented in section 2.1.1.

2.2. Acquisition of laser scanning data

2.2.1. Unmanned Laser Scanning (ULS_D)

ULS_D data, with a non-repetitive scanning pattern and discrete return, were collected in March 2021 using a GS-MID40 laser scanning sensor with a 905 nm wavelength adjusted to 160 kHz. Laser scanning was installed on an Unmanned Aerial System DJI Matrice 300 RTK, flying 100 m AGL, at a mean speed of 18 km·h⁻¹, and a scanning frequency of 200,000 points·s⁻¹. DJI Pilot software was used to conduct the flight. The GS-MID40 laser scanning

Table 1

Forest metrics from ten permanent plots in the Santa Rosa National Park Environmental Monitoring Super Site, Guanacaste Province, Costa Rica. (Source: Annual species and composition census, June 2021, Alberta Centre for Earth Observation Studies, University of Alberta, Edmonton, Canada). This table includes a new plot classification based on biomass thresholds: L1: Biomass $> 150 \text{ Mg}\cdot\text{ha}^{-1}$. L2: Biomass $115\text{--}150 \text{ Mg}\cdot\text{ha}^{-1}$. I: Biomass $50\text{--}115 \text{ Mg}\cdot\text{ha}^{-1}$. E: Biomass $< 50 \text{ Mg}\cdot\text{ha}^{-1}$.

Plot	Age	Plot Area m^2	Tree Density $\text{trees}\cdot\text{ha}^{-1}$	Dominant Height m	Basal Area $\text{m}^2\cdot\text{ha}^{-1}$	HCI	Biomass $\text{Mg}\cdot\text{ha}^{-1}$
Late 1 (L1.2)	> 90	1000	1450 ± 350	20 ± 3.4	38.5 ± 0.5	132	171.7
Late 1 (L1.1)	> 90	1000	1390 ± 350	18 ± 3.1	29.2 ± 0.3	116	156
Late 2 (L2.3)	> 90	1000	1010 ± 350	20 ± 3.9	28.8 ± 0.6	58.2	122.2
Late 2 (L2.2)	> 90	10000	684 ± 350	21.5 ± 4.0	17.2 ± 0.1	25.3	129.5
Late 2 (L2.1)	> 90	1000	1090 ± 350	22 ± 3.6	29.2 ± 0.7	69.8	118.8
Intermediate (I3)	~ 50	1000	690 ± 232	16 ± 3.2	17.6 ± 0.3	19.8	74.3
Intermediate (I2)	~ 50	1000	1140 ± 232	20 ± 3.1	28.5 ± 0.5	32.5	52.4
Intermediate (I1)	~ 51	1000	1220 ± 232	12 ± 2.1	15.1 ± 0.3	22.1	51
Early (E2)	~ 30	1000	1190 ± 182	10 ± 1.4	6.8 ± 0.1	7.3	20.7
Early (E1)	~ 30	1000	890 ± 182	8.0 ± 1.4	8.2 ± 0.1	8.1	22.5

system integrates the Livox MID40 laser head, IMU, and GNSS into a single platform. A point cloud was also obtained at our study site, with a minimum (mean) density of $800 \text{ points}\cdot\text{m}^{-2}$ (fig. 3 left).

2.3. Discrete Airborne Laser Scanning (ALS_D)

The ALS_D data, with a repetitive linear scanning pattern and discrete return, were collected in May 2021 using a Riegl LMS Q680i laser scanning sensor with a wavelength of 1,550 nm. The sensor was adjusted to 400 kHz and installed on a Piper PA-23-250 Azteca D aircraft flying 500 m above ground level (AGL) at a mean speed of $158 \text{ km}\cdot\text{h}^{-1}$ and scanning frequency of $266,000 \text{ points}\cdot\text{s}^{-1}$. The LiteMapper IGI 6800i system was used for flight, which integrates various components into a single platform: the Riegl LMS Q680i laser scanning system, DigiCAM H5D-50 photogrammetric camera, inertial measurement unit (IMU), and global navigation satellite system (GNSS), equipped with an electronic device to offset the image drag and a microprocessor for the automatic control of exposure. Navigation and inertial systems were integrated into this system. A point cloud was obtained with a minimum (mean) density of $12 \text{ points}\cdot\text{m}^{-2}$ (fig. 3 right).

2.3.1. Space Laser Scanning (SLS_{FW}) Data

Acquisitions from GEDI have been conducted over our study area since 2019. This instrument, capable of recording full-waveform laser scanning data, is installed in the International Space Station and thereby maintains an ongoing record of the Earth's surface between the latitudes of 51.6°N and 51.6°S (Dubayah et al., 2020). The laser pulses emitted by the GEDI have a wavelength of 1,064 nm and can emit $242 \text{ pulses}\cdot\text{s}^{-1}$ with a footprint of 25 m. The data provided by the GEDI were downloaded at three product levels for this study: L1B, L2A, and L2B. The L1B data consist of geolocated waveforms at a footprint diameter of 25 m ($\sim 82 \text{ ft}$). The L2A products are built upon the raw waveforms to derive ground elevation, canopy top height, and relative height (RH) metrics. The L2B products further extract biophysical variables, including the canopy cover fraction (CCF), CCF profile, leaf area index (LAI), and LAI profile from the full-waveform data. In addition to these levels, GEDI offers L1A products (raw waveforms), L3 products (gridded Level 2 metrics at 1 km), L4A products (footprint-level aboveground biomass), and L4B products (gridded aboveground biomass density).

2.4. Processing the laser scanning data

Figure 4 shows the methodological workflow used for processing the ALS_D , ULS_D , and SLS_{FW} data. Calculating the laser scanning trajectory, both ALS_D and ULS_D involve a differential adjustment of the aircraft's position and orientation system (POS) and the UAV system with the integration of Global Navigation Satellite System (GNSS) base stations on the ground. The Continuously Operating Reference Stations (CORS) of [Costa Rica's National Geographic Institute](#) were used. This made it possible to adjust the trajectory followed by the aircraft, which was recorded through

Table 2

Forest metrics derived from ALS_D and ULS_D laser scanning data using the CloudMetrics module in FUSION/LDV. Fusion computes statistics using elevation (Elev) and intensity (Int) values for each sample.

Metric	Description
Total return count	Total number of returns
Return count	Count of returns by return number (support for up to 9 discrete returns)
Elev minimum / Int minimum	Minimum
Elev maximum / Int maximum	Maximum
Elev mean / Int mean	Mean
Elev median / Int median	Median (output as 50th percentile)
Elev mode / Int mode	Mode
Elev stddev / Int stddev	Standard deviation
Elev variance / Int variance	Variance
Elev CV / Int CV	Coefficient of variation
Elev IQ / Int IQ	Interquartile distance
Elev skewness / Int skewness	Skewness
Elev kurtosis / Int kurtosis	Kurtosis
Elev AAD / Int AAD	Average absolute deviation (AAD)
Elev MAD median	MADMedian (median of the absolute deviations from the overall median)
Elev MAD mode	MADMode (median of the absolute deviations from the overall mode)
Elev L / Int L	L-moments (L1, L2, L3, L4)
Elev L skewness / Int L skewness	L-moment skewness
Elev L kurtosis / Int L kurtosis	L-moment kurtosis
Elev P / Int P	Percentile values (1st, 5th, 10th, 20th, 25th, 30th, 40th, 50th, 60th, 70th, 75th, 80th, 90th, 95th, 99th percentiles)
Canopy relief ratio	(mean – min) / (max – min)
Elev SQRT mean SQ, Elev CURT mean	Generalized means for the 2nd and 3rd power (quadratic and cubic means)
CUBE	

an aeronautical-grade airborne GNSS receptor that marks the position of the aircraft, as it provides the position for the laser scanning sensor, thus making it possible to record the data collection position in real time.

The combined use of Aeroforce, [Grafnav](#) and Inertial Navigation System (INS) Shuttle [Trajectory](#) was applied in this study to process the laser scanning trajectories. Once the data were extracted from the inertial navigation system and converted into a legible format, the differential GNSS trajectory obtained was analyzed considering the number of satellites received in the observation and the precision in the XYZ coordinates of each trajectory point. Calculation of the trajectory was smoothed with data from the Inertial Measurement Unit (IMU), thus making the Differential Global Positioning System (DGPS) estimate more accurate and robust. Two files were obtained from the DGPS/POS calculation process: one as a solution ‘.pof/sbet’, which contains all information corresponding to the trajectory, and another ‘.txt/out’ with coordinates, translations, rotations, and shifts.

Along with processing data related to the position and orientation of the sensor, leading to the calculation of the trajectory, post-processing was performed on the data collected by the laser sensor to obtain the required LAS/LAZ point cloud and additional information necessary for subsequent processing (filtering, classification, display, etc.). The post-processing phase of the raw laser data was performed using software provided by the manufacturers of the Riegl and Geosun laser scanning systems. Binary files in LAS format (LASer) were obtained from data processing, which contained information on the horizontal and vertical coordinates of the laser scanning point cloud, as well as additional supplementary information, such as intensity and returns.

The last stage involved preparing data using [LAStools software](#), wherein the following processes were applied: (i) creation of 125×125 m tiles, (ii) detection and elimination of duplicate points, (iii) detection and elimination of noise, (iv) detection and elimination of outliers, (v) coherence in Z, GPS time, and returns; (vi) classification of the point cloud into two categories: ground and non-ground; (vii) height normalization; and (viii) cropping the point clouds with the polygons of the plots. Finally, forest metrics were extracted (table 2) for all plots using the LAS point clouds normalized with [FUSIONLDV software](#) (McGaughey, 2021).

To process the SLS_{FW} data, we used the **rGEDI R package** for visualization and analysis (Silva et al., 2018). This package facilitated the acquisition of GEDI data for the study area. Eleven (11) GEDI datasets were obtained and examined in this study. Upon reviewing the metadata associated with the GEDI information, it was discovered that all datasets had a quality flag value of zero (0), signifying that the available data were of poor quality. A quality flag value of zero (0) indicates that the laser shot fails to meet the established criteria based on energy, sensitivity, amplitude, and real-time surface monitoring quality. As an alternative, the NASA GEDI simulator (Hancock et al., 2019) in the R language was used to reproduce the full-waveform data based on the ALS_D data (fig. 5) and extract forest metrics (table 3).

Table 3: Metric names and statistics using GEDI full-waveform signal values. Forest metrics derived from SLS_{FW} laser scanning data. Source: (i) (Hancock et al., 2019). GEDI simulator: **A large-footprint waveform lidar simulator for calibration and validation of spaceborne missions. Earth and Space Science**; (ii) **gediSimulator**

Metric Abbreviation	Metric Description
gHeight	Ground elevation (m) from Gaussian fitting
maxGround	Ground elevation (m) from lowest maximum
inflGround	Ground elevation (m) from inflection points
signal top	Elevation of first point above noise (may include noise tracking)
signal bottom	Elevation of last return above noise (may include noise tracking)
cover	Canopy cover (fraction) from area of Gaussian fitted ground. Uses $\rho_v = 0.57$ and $\rho_g = 0.4$
leading edge ext	Leading edge extent (m), from Lefsky et al. (2007)
trailing edge extent	Trailing edge extent (m), from Lefsky et al. (2007)
rhGauss	0–100 RH metrics, Gaussian method
rhMax	0–100 RH metrics, maximum method
rhInfl	0–100 RH metrics, inflection method
gaussHalfCov	Canopy cover (fraction) from double the energy beneath Gaussian ground
maxHalfCov	Canopy cover (fraction) from double the energy beneath lowest maximum ground
infHalfCov	Canopy cover (fraction) from double the energy beneath inflection ground
bayHalfCov	Canopy cover (fraction) from double the energy beneath Bayesian ground
lon	Footprint centre longitude in ALS projection (m)
lat	Footprint centre latitude in ALS projection (m)
waveEnergy	Total energy within waveform (scaled by noise in simulations)
blairSense	Blair's sensitivity metric (canopy cover at which SNR reaches 90)
FHD	Foliage height diversity
niM2	Ni's biomass metric: sum of RH metrics ²
niM2.1	Ni's biomass metric: sum of RH metrics ^{2.1}
wave ID	Waveform label, relates to plot name and footprint number
true ground	Ground elevation (m) from ALS, centre of gravity of ground points
true top	Elevation of highest point of waveform (m), without noise
ground slope	Effective ground slope (degrees), from width of ground return
ALS cover	Canopy cover (fraction) from ALS data ($\rho_v = 0.57$, $\rho_g = 0.4$)
rhReal	0–100 RH metrics, real data
groundOverlap	Fraction of ground return overlapping with canopy return (understorey measure)
groundMin	Depth of minimum between ground and canopy return (understorey measure)
groundInfl	Second derivative at inflection point between ground and canopy return (understorey measure)
pointDense	Average ALS point density within GEDI footprint
beamDense	Average ALS beam density within GEDI footprint

2.5. Regression models

To estimate Above Ground Biomass (AGB), we implemented two distinct regression approaches: Ordinary Least Squares (OLS) and Support Vector Machine (SVM) regression. These models were developed to evaluate and compare AGB estimates derived from metrics extracted from three different laser scanning systems: (ALS_D), (ULS_D), and (SLS_{FW}).

The dependent variable (AGB) was calculated using field measurements from the 2021 Forest Inventory, whereas the independent variables consisted of metrics derived from each laser scanning system. Model development and evaluation were performed using the [Weka machine learning framework](#); (Frank et al., 2016), a comprehensive suite of algorithms for data mining tasks.

The modeling workflow (fig. 6) encompassed the following:

- Feature extraction from each laser scanning dataset
- Data preprocessing and normalization
- Model training using both OLS and SVM approaches
- Cross-validation for model assessment
- Performance evaluation using standard regression metrics

This methodological approach allowed us to systematically compare the effectiveness of different laser scanning systems and regression techniques for estimating above-ground biomass (AGB) in forest environments.

2.6. Exploratory data analysis

Height and/or diameter at breast height (DBH) at the plot level, obtained from the 2021 forest inventory, were used in the AGB modeling. Following the standard Discrete Approach (DA), total AGB was calculated at the plot level by summing the biomass of all trees within the plot, as determined using Equation (1). Subsequently, the mean tree-level AGB (AGB_m) was derived by dividing the total plot-level AGB by the number of trees within the plot. This method aligns with established practices in forest inventories, as described by Chave et al. (2014), and is widely used to connect tree-level measurements to regional AGB estimates. The DA provides a reliable framework for biomass estimation, although it may underestimate biomass near plot boundaries compared to alternative methods such as the Continuous Approach (CA).

For the laser scanning metrics, two conditions were checked: variance and correlation (fig. 7). All metrics with a variance of zero were discarded. Subsequently, a correlation analysis was performed on the remaining variables. Variables with a low Pearson's correlation (ρ) of less than 0.5 were preferred, so they describe the variance of the AGB in the population. According to Gevrey et al. (2003), variables with a range of relative importance greater than 0.5 are the most important. This importance classification was used as a guide to select the three most important variables when none reached 0.5.

The criteria for the selection of regression variables were the correlation and significance of the parameters associated with each variable. The criterion for model selection was the evaluation of the error and coefficient of determination (R^2). In this case, R^2 is the square of Pearson's correlation coefficient, which is applicable only for OLS (simple linear regression).

2.7. AGB Modeling

The above-ground biomass (AGB) was modeled using two algorithms: Ordinary Least Squares (OLS) regression and Support Vector Machines (SVM). Equation (2) was used to define the relationship between AGB and forest metrics derived from the laser scanning data:

$$AGB = f(LS) \quad (2)$$

In this equation, AGB represents the above-ground biomass, and LS refers to the set of forest metrics derived from the ALS_D , ULS_D , and SLS_{FW} data. This equation generally applies to both OLS and SVM approaches as a framework for relating AGB to laser scanning metrics. The importance of the variables within the laser scanning metrics was determined using the generalized additive model (GAM) algorithm implemented via the `VarImp` function from the `caret` library in R. This step identified the laser scanning metrics that contributed most significantly to explaining AGB variability and was used to guide model development and refinement.

2.7.1. OLS Algorithm

The forest metrics obtained from the laser scanning data were analyzed as independent variables using the search algorithms *Wrapper Subset Evaluator* and *Attribute Subset Evaluator* within the Weka machine learning framework. The selected variables were entered into simple linear regression equations, and regression parameters were obtained to determine AGB . The data were then validated using information from each plot by calculating the total above-ground biomass (AGB_t) and mean above-ground biomass (AGB_m), and the results were compared with the forest inventory data.

2.7.2. SVM Algorithm

The Support Vector Machine (SVM) algorithm was applied to model the AGB using laser scanning metrics. To ensure the reproducibility of the analysis, the random seed was set to 123. The available data were divided into two portions: a training dataset (80%) for model development and a test dataset (20%) for model evaluation. The machine learning algorithm implementation followed the methodology described by Torre-Tojal et al. (2022), who demonstrated its effectiveness in processing LiDAR-derived metrics for biomass estimation.

Hyperparameter tuning was conducted to optimize the performance of the SVM regression model following a systematic approach similar to that described by Yan et al. (2024). A grid search approach was used to systematically explore combinations of hyperparameters. Specifically, the σ parameter was varied from $1/5$ to $1/4$ to 2 , and the cost parameter C was varied from 1 to 5 . To enhance the robustness and reliability of the model, cross-validation was performed using a scheme that incorporated randomized replacements, building upon the machine learning framework established by Xu et al. (2024). This approach involved training the model on eight plots and validating it on two plots, repeated nine times with different randomized selections of the training and validation datasets.

This modeling process was applied separately to estimate AGB_t and AGB_m . Each iteration of the cross-validation process generated a set of optimized hyperparameter values and corresponding biomass estimates. This approach ensured that the SVM algorithm was systematically calibrated and evaluated, enabling it to effectively predict AGB using laser scanning metrics, consistent with the findings of Torre-Tojal et al. (2022). The results of this process provide critical insights into the model's performance and its ability to generalize to new, unseen data.

2.7.3. Model Fit: Underfitting vs. Overfitting

Underfitting and overfitting are common challenges in regression modeling, as they can lead to poor generalization and unreliable predictions (Ghojogh and Crowley, 2019). To ensure a well-fitted model, we employed the following strategies:

- **Hyperparameter Grid Search with Nested Cross-Validation:** We utilized the *caret* package (Kuhn, 2019) to perform a systematic grid search for hyperparameter tuning. This approach incorporates nested cross-validation to minimize bias and variance, ensuring robust model evaluation.
- **Balanced Selection of Important Variables:** The model was designed to include a balanced number of important variables, as suggested by Duncanson et al. (2022). This step helped prevent overfitting by avoiding an overly complex model structure.
- **Avoidance of Extreme Hyperparameter Values:** Hyperparameter search values were carefully selected to avoid extreme levels, following the recommendations of Laref et al. (2019). This ensured that the model remained stable and avoided overfitting owing to excessively high or low parameter values.

These measures collectively ensure that the model achieves an optimal balance between bias and variance, thereby improving its ability to generalize to unseen data.

2.8. Estimate of carbon in reservoirs

Above-ground biomass (AGB) was converted into carbon (C) using equation (3), with a mean carbon content of 47%, as reported for tropical forest wood by Calvo-Rodriguez et al. (2021). This percentage represents the average proportion of carbon stored in the dry biomass of tropical trees, making it a critical factor for estimating carbon stocks in forest ecosystems. This conversion is based on the assumption that nearly half of the dry biomass in tropical forests is composed of carbon, a value widely accepted in ecological and forestry studies.

$$C = AGB \times 0.47 \quad (3)$$

To calculate the carbon dioxide equivalent (CO_2e), as indicated by the Intergovernmental Panel on Climate Change (IPCC), equation (4) was used:

$$CO_2e = k_r \times C \quad (4)$$

Where CO_2e is the carbon dioxide equivalent or fixed, C represents carbon, and k_r has a value of 3.67, which is the conversion factor derived from the molecular weights of carbon dioxide (44) and carbon (12).

2.9. Evaluation of results

The regression percentage error was used to select the best regression model under the OLS or SVM frameworks. This error is obtained by calculating the difference between the estimated AGB values from the forest metrics extracted from the laser scanning data and the AGB values from the forest inventory. The best regression was expected to have an error closest to zero. Differences between the models were also evaluated by measuring the level of error using the Mean Absolute Error (MAE) and the Root Mean Square Error (RMSE). The mean absolute error was calculated as the average of the absolute errors:

$$MAE = \frac{1}{n} \sum_{i=1}^n |y_i - x_i|,$$

where y_i is the prediction and x_i is the true value. The RMSE is defined as:

$$RMSE = \sqrt{\frac{1}{n} \sum_{i=1}^n (y_i - x_i)^2},$$

which evaluates the quality of an estimator or set of predictions in terms of its variation and degree of bias.

3. Results

Our findings demonstrate the effectiveness of different LiDAR scanning approaches and regression models in estimating above-ground biomass (AGB). The Support Vector Machine (SVM) regression model showed superior performance compared to traditional Ordinary Least Squares (OLS), particularly in capturing nonlinear relationships in the data.

3.1. Exploratory Analysis, Variable Selection, and Predictive Significance

The research used 2021 forest inventory data on tree height and diameter at breast height (DBH) to model the above-ground biomass (AGB) using equation (1). A standard Discrete Approach (DA) was applied: the total AGB at each plot was calculated by summing the biomass of all individual trees, and the mean tree-level AGB was then derived by dividing the total plot-level AGB by the number of trees. fig. 8 shows the values obtained from the inventory of DBH, height, and AGB for the plots in this study.

This study examined 40 variables for ALS_D and 41 for ULS_D . In both cases, 31 variables were excluded because of high correlation, whereas six variables with low correlation ($r < 0.5$) were incorporated into the model. For ALS_D , the accepted variables were `Elev.minimum`, `Elev.mode`, `Elev.kurtosis`, `Elev.MAD.median`, `Elev.MAD.mode`, and `Elev.L3`. Similarly, for ULS_D , 31 variables were rejected because of their high correlation and six were included. The selected variables for ULS_D were `Elev.minimum`, `Elev.maximum`, `Elev.skewness`, `Elev.MAD.median`, `Elev.MAD.mode`, and `Elev.P01`. Regarding SLS_{FW} , 145 variables were evaluated, with 44 showing no variance and 92 excluded due to high correlation. Finally, nine variables were incorporated into the model: `maxGround`, `inflGround`, `lat`, `wave_energy`, `blairSense`, `pointDense`, `gLAI0t10`, `gLAI20t30`, and `hgLAI0t10`.

3.2. Correlation analysis among variables

The correlation levels and significance of the values from the exploratory analysis are shown in figs. 9 to 11. These correlograms display the accepted forest metrics for ALS_D , ULS_D , and SLS_{FW} . Significant values are indicated by white "X" marks, and the correlations among the accepted variables are shown in the diagrams.

ALS_D Data: AGB_t and AGB_m Estimates

fig. 12(a) illustrates the variable importance for AGB_t using the ALS_D dataset. After applying a threshold of 0.5, five variables were retained: `Elev.minimum`, `Elev.L3`, `Elev.MAD.mode`, `Elev.mode`, and `Elev.MAD.median`, while one variable fell below this threshold and was removed. These five predictors demonstrated the strongest influence on the AGB_t regression. For AGB_m , the relative importance of the variables is shown in fig. 12(b). Three variables, `Elev.mode`, `Elev.MAD.mode`, and `Elev.L3` surpassed the 0.5 threshold and were chosen for the AGB_m model.

ULS_D Data: AGB_t and AGB_m Estimates

fig. 12(c) displays the variable importance for predicting AGB_t with the ULS_D dataset. Initially, applying the 0.5 cutoff left only one variable (`Elev.skewness`). To avoid underfitting, the next most influential variable (`Elev.minimum`) was also included, resulting in the selection of two predictors: `Elev.skewness` and `Elev.minimum`. For AGB_m (fig. 12(d)), three variables met the 0.5 importance threshold: `Elev.maximum`, `Elev.minimum`, and `Elev.MAD.mode`. Therefore, these were chosen as the final set of predictors for the ULS_D -based AGB_m model.

SLS_{FW} Data: AGB_t and AGB_m Estimates

fig. 12(e) shows the importance of the predictors for the simulated SLS_{FW} dataset in estimating AGB_t . Strictly applying the 0.5 cutoff led to no variables meeting the criterion. Consequently, the selection rule was adjusted to include the three most influential predictors: `PointDense`, `gLA10t10`, and `lat`. Finally, fig. 12(f) depicts the importance of the variables for AGB_m estimation using the SLS_{FW} data. Here, five variables, `lat`, `pointDense`, `inf1Ground`, `blairSense`, and `maxGround`, emerged as the most significant and were thus retained for the final model.

3.3. Observations and key discoveries

Our examination indicates that a maximum of five variables is effective for constructing SVM regression models of ALS_D , ULS_D , and SLS_{FW} from either ALS_D or ULS_D . Upon evaluating the significance of the regression variables, we found that utilizing ALS_D and ULS_D allowed for a regression analysis with up to five variables, yielding minimal regression errors below 20%.

3.4. Regression analysis

Positive correlations were found between the metrics extracted from laser scanning and the forest inventory variables, namely basal area, tree height, and DBH. Laser scanning metrics were chosen to best predict the forest variables of interest in the study area. Based on the R^2 analysis, it was possible to infer that the relationship between AGB and the metrics was not linear, as very low R^2 values were found (table 4). Therefore, R^2 analyses for the SVM were omitted.

The predictive capacities of the selected models were evaluated and compared with field measurements. fig. 13 shows that the models achieved high accuracy in predicting AGB .

3.4.1. Results from the OLS approach

The regression equations for the selected variables are presented in table 5, providing a clear understanding of how these variables relate to and help estimate AGB . These formulas offer a numerical representation of the contribution of each variable to the predictive model.

The regression equations serve as models for calculating above-ground biomass (AGB), both total (AGB_t) and mean (AGB_m), utilizing variables derived from LiDAR data across different platforms: ALS_D , ULS_D , and SLS_{FW} . The equation coefficients indicate the contribution of each variable to the model. ALS_D models incorporate variables such as `Elev.mode` and `Elev.MAD.mode`, which likely reflect height distributions and variability. These equations are relatively straightforward, suggesting that AGB can be predicted using fewer variables with airborne LiDAR. ULS_D models also include `Elev.L3`, possibly representing a height percentile or other spatial characteristic, indicating that unmanned platforms capture additional details. These equations are slightly more intricate than the ALS_D models. SLS_{FW} models incorporate variables such as `maxGround`, `infGround`, and `waveEnergy`, reflecting a comprehensive structural analysis. These equations are more complex, with additional variables included to account for localized structure and variability.

Table 5: Regression equations for OLS

LiDAR	Model	Equation
ALS	AGB_t	$11833.5287 \cdot \text{Elev.mode} + 15833.2144 \cdot \text{Elev.MAD.mode} - 21535.7042$
ALS	AGB_m	$67.2704 \cdot \text{Elev.mode} + 90.5046 \cdot \text{Elev.MAD.mode} + 99.1384$

LiDAR	Model	Equation
ULS	AGB_t	$16438.5907 \cdot \text{Elev.mode} + 22310.6709 \cdot \text{Elev.MAD.mode} + 90103.6084 \cdot \text{Elev.L3} - 60521.0596$
ULS	AGB_m	$117.262 \cdot \text{Elev.mode} + 160.8225 \cdot \text{Elev.MAD.mode} + 978.146 \cdot \text{Elev.L3} - 324.0785$
SLS	AGB_t	$57496.9707 \cdot \text{maxGround} - 988867.5126 \cdot \text{infGround} - 42.0993 \cdot \text{lat} + 35386015351.4827 \cdot \text{waveEnergy} + 27763599.5646 \cdot \text{blairSense} - 2084.1821 \cdot \text{pointDense} + 38647063.6238 \cdot \text{gLAI20t30} - 35362492243.3189$
SLS	AGB_m	$379.8023 \cdot \text{maxGround} - 4056.4243 \cdot \text{infGround} - 0.262 \cdot \text{lat} + 326584097.0663 \cdot \text{waveEnergy} + 395632.1065 \cdot \text{blairSense} - 23.6081 \cdot \text{pointDense} + 269049.7965 \cdot \text{gLAI20t30} - 326668325.8232$

3.4.2. Results from the SVM approach

A grid search method was employed to identify the optimal hyperparameters that minimized the estimation error. Figure 14 illustrates the error progression during this optimization phase, depicting how the adjustments to the hyperparameters impacted the model's precision.

The analysis highlights the differences in performance across the three LiDAR platforms (ALS, ULS, and SLS) when estimating AGB using SVM. For both AGBt (total biomass) and AGBm (mean biomass), the RMSE decreased rapidly as sigma increased—particularly for ALS—up to approximately 1, after which it stabilized. This trend suggests that moderate sigma values provide the best model generalization. For ALS, the RMSE was 18% for AGBt and 13.1% for AGBm, indicating that mean biomass estimates (AGBm) were slightly more accurate than total biomass estimates (AGBt).

For ULS, the RMSE also decreases as sigma increases; however, the results are generally more sensitive to cost values. Higher cost values (e.g., lines 4 and 5 in the plots) tend to yield better performance at lower sigma levels. The RMSE for ULS is 18.6% for AGBt and 12.2% for AGBm, indicating that ULS performs slightly worse than ALS for total biomass but achieves comparable accuracy for mean biomass. These findings suggest that ULS models effectively balance complexity and performance, making them viable alternatives for specific applications.

SLS exhibits a distinct behavior compared to ALS and ULS. For AGBt, the RMSE fluctuates considerably at higher sigma values, suggesting potential overfitting or instability. In contrast, for AGBm, the RMSE stabilizes quickly at low sigma values and remains consistent across all cost levels. The RMSE for SLS was 17.1% for AGBt and 10% for AGBm, demonstrating that SLS provided the most accurate results, particularly for mean biomass. These findings highlight the advantages of the high resolution and precision offered by static LiDAR systems in capturing fine structural details.

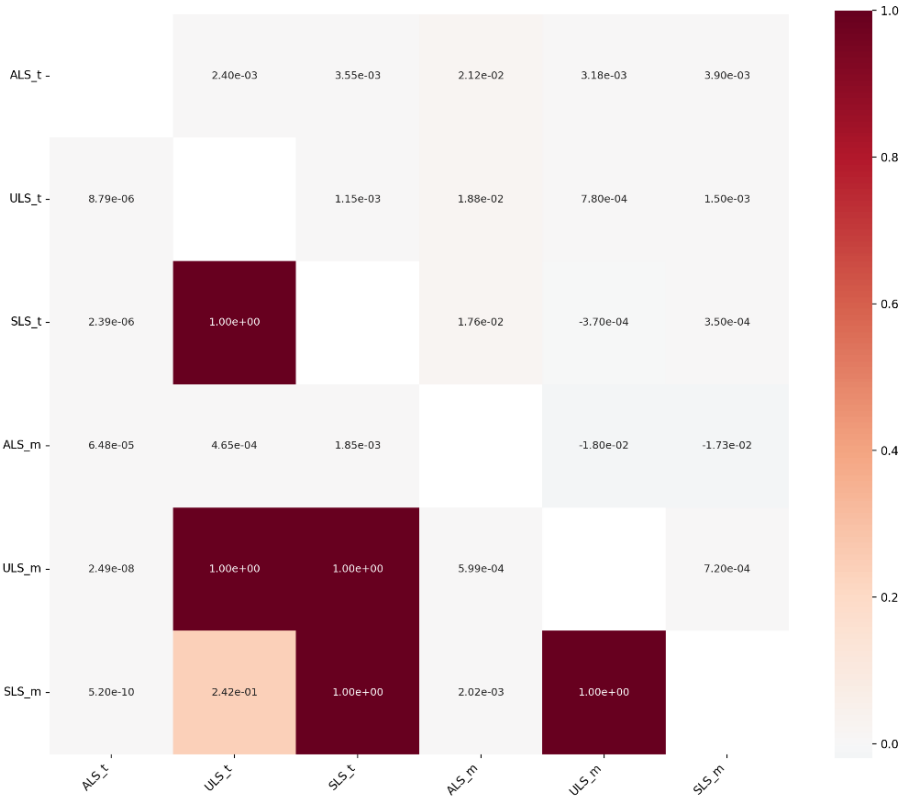
The parameter sigma plays a critical role in the SVM model by controlling the flexibility of the decision boundary. Low sigma values (e.g., < 1) produce highly complex models that may overfit the training data, whereas high sigma values (e.g., > 2) simplify the model but risk underfitting. Moderate sigma values (around 1) strike a balance between complexity and generalization, yielding the lowest RMSE across all platforms and biomass metrics. The plots indicate that this moderate sigma range consistently produced the best results.

When comparing percentage errors (e.g., 18% vs. 10%), a lower value is preferable because it indicates a smaller deviation from the true biomass. For example, the 10% error observed in SLS for AGBm was substantially better than the 18% error in ALS for AGBt. This result reflects the superior performance of SLS, particularly in mean biomass estimation, due to its ability to capture fine structural details.

The key takeaways from this analysis are as follows: SLS emerges as the most accurate platform for biomass estimation, achieving the lowest errors (17.1% for AGBt and 10% for AGBm) and excelling in small-scale, high-resolution studies thanks to its detailed structural data capture. AGBm consistently outperformed AGBt across all platforms, indicating that mean biomass is easier to estimate accurately. Moderate sigma values (approximately 1) provided the best hyperparameter settings across all platforms, striking a balance between flexibility and generalization. Finally, platform suitability depends on the scale and requirements of the study: ALS is well suited for large-scale applications owing to its simplicity and scalability; ULS is appropriate for medium-scale studies, offering a balance of mobility and precision; and SLS is unmatched for small-scale, high-accuracy research. Overall, this analysis underscores the importance of tailoring both platform selection and model configuration to the specific needs of biomass estimation projects.

The exhaustive grid search technique for hyperparameter optimization in training the SVM-based regression model yielded the optimal values summarized in table 5. The table reports performance metrics (SVMr error, expressed as a percentage) for both AGBt (total above-ground biomass) and AGBm (mean above-ground biomass), along with the corresponding optimal hyperparameter combinations (cost, c , and kernel parameter, σ) for each LiDAR platform (ALS,

Heatmap de la Matriz Rsquared

**Table 4**The differences between the models using R^2 .

ULS, and SLS). In addition, it lists the input variables that contributed most significantly to the regression models for each platform.

Table 6: Hyperparameters found for the SVM and corresponding errors for AGBt and AGBm.

LS	Metrics	SVMr error (%)	
		AGBt	AGBm
ALS	Elev.minimum, Elev.L3, Elev.MAD.mode	18.0	13.1
	Elev.mode, Elev.MAD.median	$c = 4, \sigma = 0.25$	$c = 5, \sigma = 2$
ULS	Elev.skewness, Elev.minimum	18.6	12.2
	Elev.maximum, Elev.MAD.mode	$c = 5, \sigma = 3$	$c = 5, \sigma = 0.3$
SLS	pointDense, gLAI0t10, lat	17.0	10.0
	inflGround, blairSense, maxGround	$c = 3, \sigma = 0.3$	$c = 2, \sigma = 0.2$

The analysis in table 6 highlights the performance of SVM-based regression models across the three LiDAR platforms: ALS, ULS, and SLS. For ALS, two combinations of input variables yielded strong results. For AGBt, the best-performing variables were *Elev.minimum*, *Elev.L3*, and *Elev.MAD.mode*, whereas for AGBm, the most effective variables were *Elev.mode* and *Elev.MAD.median*. The estimation error (SVMr error) for AGBt was 18.0%, while for AGBm it was 13.1%, indicating that mean biomass is easier to estimate using ALS data. The optimal hyperparameters for ALS were $c = 4, \sigma = 0.25$ for AGBt, and $c = 5, \sigma = 2$ for AGBm.

For ULS, the key variables for AGBt were *Elev.skewness* and *Elev.minimum*, whereas *Elev.maximum* and *Elev.MAD.mode* were the most significant for AGBm. The estimation errors for ULS were slightly higher than those for ALS, with AGBt at 18.6% and AGBm at 12.2%. The optimal hyperparameters for ULS were $c = 5$, $\sigma = 3$ for AGBt and $c = 5$, $\sigma = 0.3$ for AGBm.

SLS exhibited the best performance among the three platforms. The key variables for AGBt were *pointDense*, *gLAI0t10*, and *lat*, whereas *inflGround*, *blairSense*, and *maxGround* were the most significant for AGBm. The estimation errors for SLS were the lowest, at 17.0% for AGBt and 10.0% for AGBm. The optimal hyperparameters for SLS were $c = 3$, $\sigma = 0.3$ for AGBt and $c = 2$, $\sigma = 0.2$ for AGBm.

The parameters sigma (σ) and cost (c) play critical roles in the performance of the SVM model. Sigma controls the flexibility of the decision boundary. Low sigma values ($\sigma < 1$) produce highly complex decision boundaries that may lead to overfitting, whereas high sigma values ($\sigma > 2$) create smoother boundaries that may result in underfitting. Moderate sigma values ($\sigma \approx 0.25$ to $\sigma \approx 0.3$) provide the best balance between complexity and generalization across all platforms.

The cost parameter determines the trade-off between minimizing training error and maintaining a simple model. High cost values ($c > 3$) penalize errors more strongly, leading to models that fit the training data tightly, whereas low cost values ($c < 3$) allow for greater flexibility and often generalize better. Higher cost values are more effective for ALS and ULS, while lower cost values perform well for SLS.

SVM regression was then conducted using the identified hyperparameters, and the resulting estimates were compared against the forest inventory for both AGBt and AGBm. fig. 15 provides a synthesized view of the percentage errors, highlighting both the discrepancies and the accuracy of the model predictions.

The error differences between ALS and ULS for both AGBt and AGBm estimates are minimal, indicating comparable performance of these platforms in most cases. However, slight variations were observed in specific plots, such as L2.2, where ULS exhibited marginally higher errors. Errors from the SLS platform, particularly for AGBt, were also slightly higher in certain plots, including L2.2 and L2.3. This may be attributed to the greater sensitivity of SLS to structural variations in denser or more complex vegetation types.

The highest error for AGBt, observed in plot L2.2, exceeded 90% for both ALS and ULS, highlighting a significant limitation in estimating total biomass for that specific plot. Such errors may stem from structural complexities or inaccuracies in the input data. For AGBm, the highest error was considerably lower than that of AGBt, peaking at 50% in plot L2.2 with SLS. This demonstrates that mean biomass is generally easier to estimate accurately than total biomass, as it reduces variability and noise in the data.

The lowest errors were observed for SLS in plots L1.1 and L1.2, where AGBt and AGBm errors consistently ranged between 3–5%. Notably, ULS_D also achieved very low errors in plot I1 for AGBm, with a value of 0.6%. This suggests that ULS can achieve high precision under certain conditions, particularly in areas with lower structural complexity.

Across all platforms, AGBm estimates consistently exhibited lower errors than AGBt, underscoring the challenges of modeling total biomass due to its reliance on aggregated structural metrics. Certain plots, such as L2.2, emerged as outliers with substantially higher errors across all platforms, highlighting the importance of identifying and addressing plot-specific factors—such as atypical vegetation structures or measurement inconsistencies—that may drive these deviations.

ALS performed well in most plots but showed elevated errors in complex cases like L2.2 for AGBt. ULS maintained performance comparable to ALS but occasionally exhibited slightly higher errors in challenging plots. SLS produced precise estimates in simpler plots (e.g., L1.1 and L1.2) but struggled in more complex plots such as L2.2, for both AGBt and AGBm.

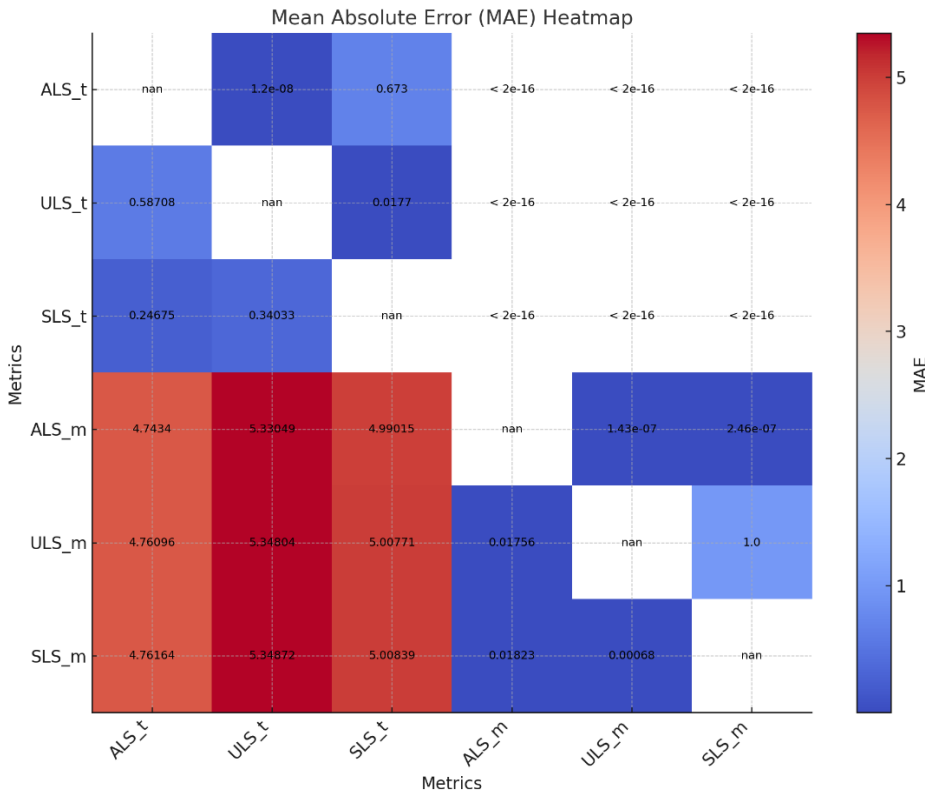
3.5. Comparison between OLS and SVM AGB Estimates

The Mean Absolute Error (MAE) heatmap provides valuable insights into the variability of biomass estimates and their associated errors. As shown in table 7, the differences in biomass estimates are directly correlated with the magnitude of error observed in the measurements or calculations. The upper diagonal of the table quantifies these errors, offering a clear view of how inaccuracies can propagate and lead to discrepancies in the final biomass estimates. The lower section of the same table reports the statistical significance of these variations, indicating the confidence levels associated with each comparison.

The lowest error for AGBt was observed between ULS_D and SLS_{FW} estimations, with a value of 0.34033 Mg ha⁻¹, indicating that the two datasets are highly compatible for estimating total biomass. For AGBm, the error between the ALS_D and ULS_D estimates was 0.01756 Mg ha⁻¹, which was notably lower than the error observed between ALS_D

Table 7

Differences between models using MAE. p-value adjustment: Bonferroni. Upper part of the diagonal: estimates of the difference. Lower part of the diagonal: p-value for H_0 : Difference = 0.



and SLS_{FW} ($-0.24675 \text{ Mg ha}^{-1}$). This demonstrates the strength of the ALS_D and ULS_D data for mean biomass estimation, while highlighting a relatively higher discrepancy when comparing ALS_D with SLS_{FW} .

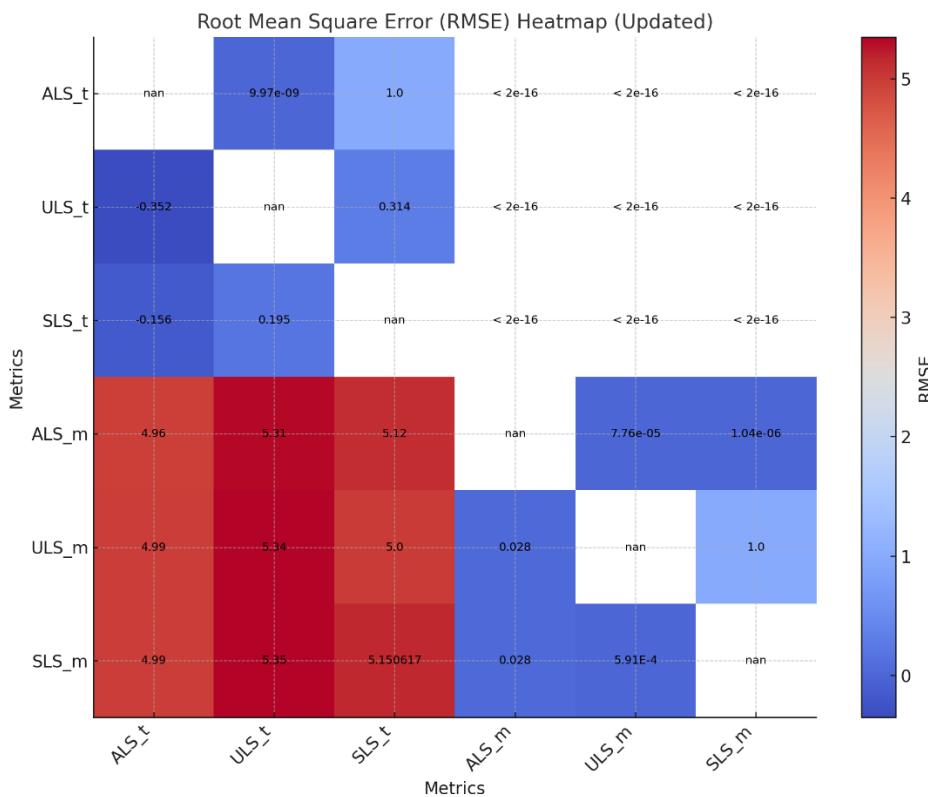
Interestingly, we found insufficient evidence to support a direct comparison between SLS_{FW} and ULS_D for AGBm estimations. This lack of statistical evidence suggests potential limitations in modeling or inherent variability between the two datasets that prevent robust comparisons. Similarly, for AGBt estimations, insufficient evidence was found to compare SLS_{FW} and ALS_D estimates, which may reflect the higher sensitivity of total biomass calculations to structural differences in the data.

The results confirm that AGBt can be estimated effectively using both ALS_D and ULS_D , and that ULS_D data can be reliably modeled from SLS_{FW} with low error and high confidence. However, direct comparisons between SLS_{FW} and ALS_D remain inconclusive for AGBt estimates. For AGBm, the results are more consistent, with ALS_D yielding similar estimations when compared to ULS_D and SLS_{FW} . Nevertheless, no evidence was found to support a direct comparison between SLS_{FW} and ULS_D for mean biomass.

As shown in Table 8, the maximum percentage error observed in AGB modeling reached 92.7% for AGBt on plot L2.2 when utilizing ULS_D data. Similarly, the most substantial modeling error for AGBm was 46.4%, recorded on the L2.2 plot using SLS_{FW} data. In a broader context, the estimation errors for AGB were higher in L2.1 and L2.2 late-stage plots compared to L1.2, L1.1, and early and intermediate plots (E and I). The differences found in the AGB regression when using ALS_D or ULS_D data were relatively low, and the differences between the mean errors of ALS_D and ULS_D with the SLS_{FW} data only reached 0.92% of the mean errors for AGBm and 0.68% for AGBm. The accuracy of AGB modeling using SVM exceeded 81% (ALS_D : 82.0%, ULS_D : 81.4%, and SLS_{FW} : 82.9%), whereas the accuracy of OLS modeling was approximately 60%.

Table 8

Differences between models using RMSE.



3.6. Results of AGB estimates for Forest Inventory, ALS_D , ULS_D , and SLS_{FW}

Figure 16 shows the estimates obtained using the SVM for AGBt and AGBm across the 10 plots. The AGB values were predicted using laser-scanning metrics, with the best estimates achieved using the SLS_{FW} data.

Fig. 17 demonstrates the relationship between predicted above-ground biomass (AGB) and inventory-based AGB, expressed in $Mg\ ha^{-1}$, across three LiDAR systems (ALS_D , ULS_D , and SLS_{FW}) and different forest successional stages (Early, Intermediate, and Late). The x-axis represents the inventory-derived AGB values, considered the ground truth, whereas the y-axis displays the AGB predicted using the three LiDAR systems. A dashed diagonal line (1:1 line) is included to represent perfect agreement between the predicted and inventory-based AGB. The closer the points and trend lines are to this diagonal, the greater the prediction accuracy.

Color-coded lines correspond to forest successional stages: red for early successional forests, green for intermediate forests, and blue for late successional forests. These lines illustrate the trend of predicted AGB across stages, while the shaded areas around them represent confidence intervals. Narrower shaded regions indicate greater prediction confidence, whereas wider intervals reflect higher variability or uncertainty in the predictions. Late successional plots consistently exhibited the highest AGB values, as indicated by the blue lines, aligning with their advanced forest structure and higher biomass. Intermediate and early-stage plots showed lower AGB values, consistent with their respective stages of forest development.

The markers on the lines represent predictions from different LiDAR systems. Circles correspond to ALS_D , triangles to SLS_{FW} , and squares to ULS_D . The positions of these markers along the lines provide insight into how each system performs across successional stages. For instance, ALS_D and ULS_D predictions are closely aligned with the 1:1 line, particularly in intermediate- and late-stage forests, indicating high prediction accuracy. SLS_{FW} demonstrates slightly greater variability but remains accurate, especially in late-successional forests where AGB values are the highest.

In terms of overall accuracy, the late-stage forests exhibited the highest biomass values, ranging from 26.0 Mg ha⁻¹ to 175.4 Mg ha⁻¹, as predicted by all systems. The accuracy of the three LiDAR systems is reflected in their percentage agreement with inventory-based values, with SLS_{FW} achieving the highest accuracy (82.9%), followed by ALS_D (82.0%) and ULS_D (81.4%). This analysis underscores the reliability of all three systems for AGB estimation in tropical forests, with only minor variations between systems across different successional stages.

4. Discussion

In this study, we combined laser scanning technology with OLS and SVM regression models to evaluate the alignment between field-based aboveground biomass (AGB) estimates and LiDAR-derived mapping in a tropical dry forest in Costa Rica. Specifically, we integrated allometric equations and forest inventory data to estimate AGB for trees with diameters greater than 5 cm. This approach aimed to address the critical need, highlighted in the introduction, for more accurate and efficient methods to quantify forest carbon stocks in tropical dry forest ecosystems, which remain understudied compared with other tropical biomes.

Our results indicate that the SLS_{FW} model achieved slightly lower errors (ranging from 12.2% to 18.6%) than the ALS_D and ULS_D models. This finding suggests that full-waveform LiDAR may provide a more reliable approach for AGB estimation under certain conditions. In addition, we observed the pivotal role of the footprint center latitude (*lat*) in correcting atmospheric effects on laser pulse measurements. When this variable was excluded, the modeling errors increased dramatically from 8% to 58%, underscoring the importance of incorporating atmospheric corrections in biomass estimation for tropical forest environments.

Despite these promising outcomes, several limitations emerged. First, the sample size of ten plots posed challenges for OLS-based modeling, as it was difficult to meet all the assumptions required for parametric analyses. Second, overfitting issues were noted in the SLS_{FW} and ULS_D regressions, likely stemming from the selection of too few input variables. Future research with larger datasets and a more diverse range of ecological conditions may help address these concerns by refining model parameters and ensuring greater generalizability.

Below, we provide a deeper examination of the models, their limitations, and how our results compare with those of previous research. We then conclude with a broader perspective on how these findings contribute to advancing the objectives stated in the Introduction and to the wider field of forest carbon monitoring.

4.1. Discussion on Models and Their Limitations

Previous studies have investigated various combinations of LiDAR systems and statistical approaches for AGB estimation; however, relatively few have explicitly employed OLS and SVM together in tropical dry forests (Rathi, 2018; Schuh et al., 2020; Torre-Tojal et al., 2019). Our study addresses this gap by systematically comparing these models with different LiDAR data sources (ALS_D, ULS_D, and SLS_{FW}).

A critical methodological consideration in AGB modeling is the selection of predictor variables. Drake et al. (2003) focused on linear regression for AGB estimation but did not detail a variable selection method, potentially due to the complexity and multiple trade-offs involved. Similarly, Gleason and Im (2012) did not specify variable selection guidelines, and Ene et al. (2012) introduced simulations for incorporating LiDAR metrics into regression but did not provide an explicit stepwise or machine learning-based selection approach. Ståhl et al. (2011) and Duncanson et al. (2022) demonstrated the utility of restricting models to between one and four well-chosen variables, often involving height and tree density, to optimize predictive performance.

Consistent with these findings, we observed that different laser scanning systems prioritize distinct sets of variables. ALS_D and ULS_D metrics emphasized elevation-related characteristics of the forest canopy, whereas SLS_{FW} metrics highlighted other structural parameters unique to full-waveform data. These discrepancies underscore the importance of tailoring variable selection to the specific LiDAR technology in use.

From a statistical standpoint, our analysis revealed that OLS-based algorithms were unsuitable for modeling biomass with only ten sample plots due to violations of fundamental statistical assumptions (e.g., normality, homoscedasticity). In contrast, SVM does not require these assumptions, making it a more robust choice for small datasets or cases where the relationship between predictors and response may be highly nonlinear. Although we employed a grid search scheme to identify the optimal cost and sigma values, we recommend further validation on expanded datasets from ecologically similar areas to confirm the stability of these SVM parameters. Finally, addressing potential overfitting in SLS_{FW} and ULS_D regressions will require the careful inclusion of additional

predictor variables, possibly guided by a stepwise approach informed by variable importance metrics (García-Gutiérrez et al., 2015).

4.2. Discussion on Biomass Estimates, Errors, and Comparisons with Other Studies

Our biomass values align with estimates reported for other Neotropical dry forests, which range from approximately 39 Mg ha⁻¹ in Chamela, Mexico, to 334 Mg ha⁻¹ in Guanacaste, Costa Rica (Calvo-Rodriguez et al., 2021). We found that the accuracy of AGB estimates was strongly influenced by LiDAR-derived metrics, echoing (Silva et al., 2017), who concluded that a high pulse density is not strictly necessary to estimate or map biomass stocks in Amazonian tropical forests.

In evaluating errors, our study achieved results comparable to those reported in the literature, such as Ståhl et al. (2011), Gleason and Im (2012), and Duncanson et al. (2022). However, the lower error margins (12.2–18.6%) achieved by the SLS_{FW} approach in this study may reflect the advantages of full-waveform LiDAR in capturing complex forest structures, particularly in heterogeneous tropical dry forests. Although ALS_D and ULS_D data produced similar errors, confirming the equivalence of these technologies requires further research, particularly across different forest types and measurement scales, consistent with the cautionary note from Zolkos et al. (2013).

Our findings also reaffirm the utility of spatially explicit modeling approaches. Although pixel-based raster methods have been commonly employed (Ene et al., 2012; Gleason and Im, 2012), point-vector models have gained traction because of their capacity to retain the full resolution of LiDAR point clouds. This study demonstrated that both approaches can yield accurate results, provided that appropriate regression techniques and corrections for atmospheric effects are applied.

Regarding overfitting, we observed that SLS_{FW} and ULS_D regressions tended to rely on a small number of predictor variables. A pragmatic solution involves broadening the candidate variable pool and applying a robust stepwise selection method. Even variables with lower relative importance can occasionally enhance overall model generalization if they capture specific forest attributes not accounted for by higher-ranked metrics. Additionally, incorporating more diverse field data, both in terms of geographic extent and ecological conditions, would help validate the transferability of these SVM-based models and refine their predictive capabilities.

4.3. Final Remarks and Broader Implications

By comparing ALS_D, ULS_D, and SLS_{FW} data using both OLS and SVM regression methods, this study expands our understanding of how different LiDAR technologies can be harnessed for reliable biomass mapping in tropical dry forests. In connection with the objectives stated in the introduction, our findings highlight the critical importance of atmospheric correction (e.g., through variables such as latitude) and robust modeling frameworks (such as SVM) for capturing the spatial variability of AGB. Moreover, this study emphasizes that while OLS remains valuable under appropriate conditions, it may be less suitable when sample sizes are small or when forest structure is highly heterogeneous.

These results pave the way for more refined and scalable strategies to map biomass in other tropical dry forest regions, thereby contributing to improved carbon accounting and forest management practices. By demonstrating the utility of different LiDAR systems and modeling techniques, we provide a framework for future research aimed at integrating advanced remote sensing data with ground-based inventories. Ultimately, these efforts will enhance our capacity to monitor and conserve tropical dry forests, which play a crucial role in global carbon cycling and biodiversity conservation, further realizing the promise outlined in the introduction to bridge data gaps and improve ecological assessments in these unique and vulnerable ecosystems.

5. Conclusions

This study evaluated the effectiveness of Support Vector Machine (SVM) regression models in estimating above-ground biomass (AGB) in a tropical dry forest in Costa Rica using various laser scanning techniques. The results demonstrate that SVM regression models, combined with allometric equations and field forest inventory data, can accurately estimate AGB for small trees with diameters exceeding 5 cm. The study found that SLS_{FW}, ALS_D, and ULS_D metrics are reliable for biomass estimation, regardless of point density, scanning pattern, number of returns, or data-logging format. However, the relative importance of the variables in the AGB regression varied across the laser-scanning systems. While OLS-based algorithms proved unsuitable for biomass regression modeling with limited sample plots, SVM regression models have emerged as a valuable tool for AGB estimation in tropical dry forests. The

study's findings, although limited by their focus on a single site and small sample size, provide insights into the potential of laser scanning technology for forest biomass estimation. With errors below 19% and no significant differences in accuracy between laser scanning systems, this methodology shows promise for the inventory and monitoring of AGB changes in tropical regions, potentially supporting REDD+ monitoring efforts. Future research could benefit from expanding datasets to multiple sites and integrating GEDI data with direct observations to enhance the generalizability of results, given the small number of sample plots.

Credit Author Statement: Nelson Mattie: Conceptualization, methodology, software, formal analysis, investigation, visualization, validation, writing – original draft. Arturo Sanchez-Azofeifa: Conceptualization, methodology, investigation, writing – review & editing, supervision. Pablo Crespo-Peremarch: Conceptualization, writing – review & editing, supervision. Juan-Ygnacio López-Hernández: Methodology, writing – review & editing, visualization, software, analysis.

Declaration of Competing Interests: The authors declare that they have no known competing financial interests or personal relationships that could have appeared to influence the work reported in this paper.

Acknowledgements: The authors acknowledge the support provided by the Centre for Earth Observation Sciences, Department of Earth & Atmospheric Sciences, University of Alberta, Canada. They are also grateful for the support provided by the Earth Observation Center Hémera at University Mayor, Chile, as well as by Natural Resources Canada and the Government of Canada. The authors further acknowledge the National Aeronautics and Space Administration (NASA) and the U.S. federal government for providing the GEDI data and software packages. Finally, the authors thank Osvaldo Valeria, Professeur, Institut de recherche sur les forêts, Université du Québec, for proofreading the revised early version of the manuscript.

References

de Almeida, C., Galvão, L., Aragão, L.e., Ometto, J., Jacon, A., de Sá, F., Sato, L., Lopes, A., de A Graça, P., de J Silva, C., et al., 2019. Combining lidar and hyperspectral data for aboveground biomass modeling in the brazilian amazon using different regression algorithms. *Remote Sensing of Environment* 232. doi:[10.1016/j.rse.2019.111323](https://doi.org/10.1016/j.rse.2019.111323).

Arroyo-Mora, J., Sánchez-Azofeifa, G., Kalacska, M., Rivard, B., Calvo-Alvarado, J., Janzen, D., 2005. Secondary forest detection in a neotropical dry forest landscape using landsat 7 etm+ and ikonos imagery. *Biotropica* 37, 497–507. doi:[10.1111/j.1744-7429.2005.00068.x](https://doi.org/10.1111/j.1744-7429.2005.00068.x).

Belete, D., Manjaiah, D., 2021. Grid search in hyperparameter optimization of machine learning models for prediction of hiv/aids test results. *International Journal of Computers and Applications* 44, 1–12. doi:[10.1080/1206212X.2021.1974663](https://doi.org/10.1080/1206212X.2021.1974663).

Berninger, A., Lohberger, S., Stängel, M., Siegert, F., 2018. Sar-based estimation of above-ground biomass and its changes in tropical forests of kalimantan using l- and c-band. *Remote Sensing* 10. doi:[10.3390/rs10060831](https://doi.org/10.3390/rs10060831).

Calvo-Rodriguez, S., Sánchez-Azofeifa, G., Durán, S., Do Espírito-Santo, M., Nunes, Y., 2021. Dynamics of carbon accumulation in tropical dry forests under climate change extremes. *Forests* 12, 1–15. doi:[10.3390/f12010106](https://doi.org/10.3390/f12010106).

Cao, S., Cao, S., Yu, Q., Yu, Q., Sanchez-Azofeifa, A., Feng, J., Rivard, B., Gu, Z., 2015. Mapping tropical dry forest succession using multiple criteria spectral mixture analysis. *ISPRS Journal of Photogrammetry and Remote Sensing* 109, 17–29. doi:[10.1016/j.isprsjprs.2015.08.009](https://doi.org/10.1016/j.isprsjprs.2015.08.009).

Chave, J., Coomes, D., Jansen, S., Lewis, S., Swenson, N., Zanne, A., 2009. Towards a worldwide wood economics spectrum. *Ecology Letters* 12, 351–366. doi:[10.1111/j.1461-0248.2009.01285.x](https://doi.org/10.1111/j.1461-0248.2009.01285.x).

Chave, J., Réjou-Méchain, M., Bürquez, A., Chidumayo, E., Colgan, M., Delitti, W., Duque, A., Eid, T., Fearnside, P., Goodman, R., et al., 2014. Improved allometric models to estimate the aboveground biomass of tropical trees. *Global Change Biology* 20, 3177–3190. doi:[10.1111/gcb.12629](https://doi.org/10.1111/gcb.12629).

Crespo-Peremarch, P., 2020. Processing and analysis of airborne full-waveform laser scanning data for the characterization of forest structure and fuel properties. Ph.D. thesis.

Drake, J., Knox, R., Dubayah, R., Clark, D., Condit, R., Blair, J., Hofton, M., 2003. Above-ground biomass estimation in closed canopy neotropical forests using lidar remote sensing: Factors affecting the generality of relationships. *Global Ecology and Biogeography* 12, 147–159. doi:[10.1046/j.1466-822X.2003.00010.x](https://doi.org/10.1046/j.1466-822X.2003.00010.x).

Duan, M., Bax, C., Laakso, K., Mashhadi, N., Mattie, N., Sanchez-Azofeifa, A., 2023. Characterizing transitions between successional stages in a tropical dry forest using lidar techniques. *Remote Sensing* 15, 479. doi:[10.3390/rs15020479](https://doi.org/10.3390/rs15020479).

Dubayah, R., Blair, J., Goetz, S., Fatoyinbo, L., Hansen, M., Healey, S., Hofton, M., Hurt, G., Kellner, J., Luthcke, S., et al., 2020. The global ecosystem dynamics investigation: High-resolution laser ranging of the earth's forests and topography. *Science of Remote Sensing* 1, 100002. doi:[10.1016/j.srs.2020.100002](https://doi.org/10.1016/j.srs.2020.100002).

Duncanson, L., Kellner, J., Armston, J., Dubayah, R., Minor, D., Hancock, S., Healey, S., Patterson, P., Saarela, S., Marselis, S., et al., 2022. Aboveground biomass density models for nasa's global ecosystem dynamics investigation (gedi) lidar mission. *Remote Sensing of Environment* 270, 112845. doi:[10.1016/j.rse.2021.112845](https://doi.org/10.1016/j.rse.2021.112845).

Ene, L., Næsset, E., Gobakken, T., Gregoire, T., Ståhl, G., Nelson, R., 2012. Assessing the accuracy of regional lidar-based biomass estimation using a simulation approach. *Remote Sensing of Environment* 123, 579–592. doi:[10.1016/j.rse.2012.04.017](https://doi.org/10.1016/j.rse.2012.04.017).

Ferraz, A., Saatchi, S., Xu, L., Hagen, S., Chave, J., Yu, Y., Meyer, V., Garcia, M., Silva, C., Roswintiart, O., et al., 2018. Carbon storage potential in degraded forests of kalimantan, indonesia. *Environmental Research Letters* 13. doi:[10.1088/1748-9326/aad782](https://doi.org/10.1088/1748-9326/aad782).

Frank, E., Hall, M., Witten, I.H., 2016. Data mining: Practical machine learning tools and techniques. 4th ed., Morgan Kaufmann Publishers.

García-Gutiérrez, J., Martínez-Alvarez, F., Troncoso, A., Riquelme, J.C., 2015. A comparison of machine learning regression techniques for lidar-derived estimation of forest variables. *Neurocomputing* 167, 24–31. doi:[10.1016/j.neucom.2014.09.091](https://doi.org/10.1016/j.neucom.2014.09.091).

Gevrey, M., Dimopoulos, I., Lek, S., 2003. Review and comparison of methods to study the contribution of variables in artificial neural network models. *Ecological Modelling* 160, 249–264. doi:[10.1016/S0304-3800\(02\)00257-0](https://doi.org/10.1016/S0304-3800(02)00257-0).

Ghojogh, B., Crowley, M., 2019. The theory behind overfitting, cross validation, regularization, bagging, and boosting: Tutorial. arXiv preprint doi:[10.48550/arXiv.1905.12787](https://arxiv.org/abs/1905.12787).

Gleason, C., Im, J., 2012. Forest biomass estimation from airborne lidar data using machine learning approaches. *Remote Sensing of Environment* 125, 80–91. doi:[10.1016/j.rse.2012.07.006](https://doi.org/10.1016/j.rse.2012.07.006).

Gonçalves, F., 2014. Vertical structure and aboveground biomass of tropical forests from lidar remote sensing. Ph.D. thesis. URL: https://ir.library.oregonstate.edu/concern/graduate_thesis_or_dissertations/1n79h9029?locale=en.

Hancock, S., Armston, J., Hofton, M., Sun, X., Tang, H., Duncanson, L., Kellner, J., Dubayah, R., 2019. Gedi simulator: A large-footprint waveform lidar simulator for calibration and validation of spaceborne missions. *Earth and Space Science* 6, 294–310. doi:[10.1029/2018EA000506](https://doi.org/10.1029/2018EA000506).

Hilje, B., Calvo-Alvarado, J., Jiménez-Rodríguez, C., Sánchez-Azofeifa, A., 2015. Tree species composition, breeding systems, and pollination and dispersal syndromes in three forest successional stages in a tropical dry forest in mesoamerica. *Tropical Conservation Science* 8, 76–94. doi:[10.1177/194008291500800109](https://doi.org/10.1177/194008291500800109).

Houghton, R., Hall, F., Goetz, S., 2009. Importance of biomass in the global carbon cycle. *Journal of Geophysical Research: Biogeosciences* 114, 1–13. doi:[10.1029/2009JG000935](https://doi.org/10.1029/2009JG000935).

Hu, T., Zhang, Y., Su, Y., Zheng, Y., Lin, G., Guo, Q., 2020. Mapping the global mangrove forest aboveground biomass using multisource remote sensing data. *Remote Sensing* 12. doi:[10.3390/rs12101690](https://doi.org/10.3390/rs12101690).

Kalacska, M., Sanchez-Azofeifa, G., Calvo-Alvarado, J., Quesada, M., Rivard, B., Janzen, D., 2004. Species composition, similarity and diversity in three successional stages of a seasonally dry tropical forest. *Forest Ecology and Management* 200, 227–247. doi:[10.1016/j.foreco.2004.07.001](https://doi.org/10.1016/j.foreco.2004.07.001).

Kellner, J., Armston, J., Birrer, M., Cushman, K., Duncanson, L., Eck, C., Fallegger, C., Imbach, B., Král, K., Krůček, M., et al., 2019. New opportunities for forest remote sensing through ultra-high-density drone lidar. *Surveys in Geophysics* 40, 959–977. doi:[10.1007/s10712-019-09529-9](https://doi.org/10.1007/s10712-019-09529-9).

Koch, B., 2010. Status and future of laser scanning, synthetic aperture radar and hyperspectral remote sensing data for forest biomass assessment. *ISPRS Journal of Photogrammetry and Remote Sensing* 65, 581–590. doi:[10.1016/j.isprsjprs.2010.09.001](https://doi.org/10.1016/j.isprsjprs.2010.09.001).

Kudo, M., Kimura, K., Morishita, S., Sun, L., 2023. Efficient leave-one-out evaluation of kernelized implicit mappings, in: *Structural, Syntactic, and Statistical Pattern Recognition*, Springer. pp. 223–232. doi:[10.1007/978-3-031-23028-8_23](https://doi.org/10.1007/978-3-031-23028-8_23).

Kuhn, M., 2019. caret: Classification and Regression Training. URL: <https://CRAN.R-project.org/package=caret>. r package version 6.0-84.

Laref, R., Losson, E., Sava, A., Siadat, M., 2019. On the optimization of the support vector machine regression hyperparameters setting for gas sensors array applications. *Chemometrics and Intelligent Laboratory Systems* 184, 22–27. doi:[10.1016/j.chemolab.2018.11.011](https://doi.org/10.1016/j.chemolab.2018.11.011).

Lee, C.K.F., Song, G., M'uller-Landau, H.C., Wu, S., Wright, S.J., Cushman, K.C., Araujo, R.F., Bohlman, S., Zhao, Y., Lin, Z., Sun, Z., Cheng, P.C.Y., Ng, M.K.P., Wu, J., 2023. Cost-effective and accurate monitoring of flowering across multiple tropical tree species over two years with a time series of high-resolution drone imagery and deep learning. *ISPRS Journal of Photogrammetry and Remote Sensing* 201, 92–103. doi:[10.1016/j.isprsjprs.2023.05.022](https://doi.org/10.1016/j.isprsjprs.2023.05.022).

Li, W., Cao, S., Campos-Vargas, C., Sanchez-Azofeifa, A., 2017. Identifying tropical dry forests extent and succession via the use of machine learning techniques. *International Journal of Applied Earth Observation and Geoinformation* 63, 196–205. doi:[10.1016/j.jag.2017.08.003](https://doi.org/10.1016/j.jag.2017.08.003).

Liu, C., Sanchez-Azofeifa, A., Bax, C., 2023. Studying tropical dry forests secondary succession (2005–2021) using two different lidar systems. *Remote Sensing* 15, 4677. doi:[10.3390/rs15194677](https://doi.org/10.3390/rs15194677).

Luo, S., Wang, C., Xi, X., Nie, S., Fan, X., Chen, H., Ma, D., Liu, J., Zou, J., Lin, Y., et al., 2019. Estimating forest aboveground biomass using small-footprint full-waveform airborne lidar data. *International Journal of Applied Earth Observation and Geoinformation* 83, 101922. doi:[10.1016/j.jag.2019.101922](https://doi.org/10.1016/j.jag.2019.101922).

Luo, S., Wang, C., Xi, X., Pan, F., Peng, D., Zou, J., Nie, S., Qin, H., 2017. Fusion of airborne lidar data and hyperspectral imagery for aboveground and belowground forest biomass estimation. *Ecological Indicators* 73, 378–387. doi:[10.1016/j.ecolind.2016.10.001](https://doi.org/10.1016/j.ecolind.2016.10.001).

McGaughey, R.J., 2021. Fusion/ldv: Software for lidar data analysis and visualization [computer software]. cran.r-project.org.

Mette, T., Papathanassiou, K., Hajnsek, I., Zimmermann, R., 2003. Forest biomass estimation using polarimetric sar interferometry. European Space Agency, (Special Publication) ESA SP , 141–146doi:[10.1109/igarss.2002.1025695](https://doi.org/10.1109/igarss.2002.1025695).

Nandlall, S.D., Millard, K., 2020. Quantifying the relative importance of variables and groups of variables in remote sensing classifiers using shapley values and game theory. *IEEE Geoscience and Remote Sensing Letters* 17, 42–46. doi:[10.1109/LGRS.2019.2914374](https://doi.org/10.1109/LGRS.2019.2914374).

Narine, L., Popescu, S., Malambo, L., 2019. Synergy of icesat-2 and landsat for mapping forest aboveground biomass with deep learning. *Remote Sensing* 11, 1–19. doi:[10.3390/rs11121503](https://doi.org/10.3390/rs11121503).

Nassar, J.M., Rodríguez, J.P., Sánchez-Azofeifa, A., Garvin, T., Quesada, M., 2008. Manual of Methods: Human, Ecological and Biophysical Dimensions of Tropical Dry Forests. Instituto Venezolano de Investigaciones Científicas (Tropi-Dry/IAI). (NO se encontró un DOI; el manual está disponible en la línea en el IAI.).

Powers, J.S., Tiffin, P., 2010. Plant functional type classifications in tropical dry forests in costa rica: Leaf habit versus taxonomic approaches. *Functional Ecology* 24, 927–936. doi:[10.1111/j.1365-2435.2010.01701.x](https://doi.org/10.1111/j.1365-2435.2010.01701.x).

Ramasubramanian, K., Singh, A., 2019. Machine learning using R: With time series and industry-based use cases in R. Apress. Link.springer.com.

Rathi, P., 2018. Biomass estimation at icesat/glas footprints using support vector regression algorithm for optimization of parameters, in: *Advances in Signal Processing and Communication*. Springer, Singapore, pp. 101–111. doi:[10.1007/978-981-10-5699-4_11](https://doi.org/10.1007/978-981-10-5699-4_11).

Santos, J., Neeff, T., Dutra, L., Araujo, L., Gama, F., Elmiro, M., 2004. Tropical forest biomass mapping from dual frequency sar interferometry (x and p-bands). International Archives of Photogrammetry, Remote Sensing and Spatial Information Sciences XXXV, 1133–1136.

Schepaschenko, D., Chave, J., Phillips, O., Lewis, S., Davies, S., Réjou-Méchain, M., Sist, P., Scipal, K., Perger, C., Herault, B., et al., 2019. The forest observation system, building a global reference dataset for remote sensing of forest biomass. *Scientific Data* 6, 198. doi:[10.1038/s41597-019-0196-1](https://doi.org/10.1038/s41597-019-0196-1).

Schuh, M., Favarin, J., Marchesan, J., Alba, E., Berra, E., Pereira, R., 2020. Machine learning and generalized linear model techniques to predict aboveground biomass in amazon rainforest using lidar data. *Journal of Applied Remote Sensing* 14, 034518. doi:[10.1117/1.JRS.14.034518](https://doi.org/10.1117/1.JRS.14.034518).

Silva, C., Hudak, A., Vierling, L., Klauberg, C., Garcia, M., Ferraz, A., Keller, M., Eitel, J., Saatchi, S., 2017. Impacts of airborne lidar pulse density on estimating biomass stocks and changes in a selectively logged tropical forest. *Remote Sensing* 9. doi:[10.3390/rs9101068](https://doi.org/10.3390/rs9101068).

Silva, C., Saatchi, S., García, M., Labrière, N., Klauberg, C., Ferraz, A., Meyer, V., Jeffery, K., Abernethy, K., White, L., et al., 2018. Comparison of small- and large-footprint lidar characterization of tropical forest aboveground structure and biomass: A case study from central gabon. *IEEE Journal of Selected Topics in Applied Earth Observations and Remote Sensing* 11, 3512–3526. doi:[10.1109/JSTARS.2018.2816962](https://doi.org/10.1109/JSTARS.2018.2816962).

Ståhl, G., Holm, S., Gregoire, T., Gobakken, T., Næsset, E., Nelson, R., 2011. Model-based inference for biomass estimation in a lidar sample survey in hedmark county, norway. *Canadian Journal of Forest Research* 41, 96–107. doi:[10.1139/X10-161](https://doi.org/10.1139/X10-161).

Sun, C., Cao, S., Sanchez-Azofeifa, G., 2019. Mapping tropical dry forest age using airborne waveform lidar and hyperspectral metrics. *International Journal of Applied Earth Observation and Geoinformation* 83, 101908. doi:[10.1016/j.jag.2019.101908](https://doi.org/10.1016/j.jag.2019.101908).

Tadese, S., Soromessa, T., 2019. Above ground biomass estimation methods and challenges: A review. *Journal of Energy Technology and Policy* doi:[10.7176/jetp/9-8-02](https://doi.org/10.7176/jetp/9-8-02).

Torre-Tojal, L., Bastarrika, A., Boyano, A., Lopez-Guede, J., Graña, M., 2022. Above-ground biomass estimation from lidar data using random forest algorithms. *Journal of Computational Science* 58, 101517. doi:[10.1016/j.jocs.2021.101517](https://doi.org/10.1016/j.jocs.2021.101517).

Torre-Tojal, L., Lopez-Guede, J., Graña Romay, M., 2019. Estimation of forest biomass from light detection and ranging data by using machine learning. *Expert Systems* 36, 1–15. doi:[10.1111/exsy.12399](https://doi.org/10.1111/exsy.12399).

Xu, L., Yu, J., Shu, Q., Luo, S., Zhou, W., Duan, D., 2024. Forest aboveground biomass estimation based on spaceborne lidar combining machine learning model and geostatistical method. *Frontiers in Plant Science* 15, 1428268.

Yan, Y., Lei, J., Huang, Y., 2024. Forest aboveground biomass estimation based on unmanned aerial vehicle–light detection and ranging and machine learning. *Sensors* 24, 7071. doi:[10.3390/s24217071](https://doi.org/10.3390/s24217071).

Yang, L., Shami, A., 2020. On hyperparameter optimization of machine learning algorithms: Theory and practice. *Neurocomputing* 415, 295–316. doi:[10.1016/j.neucom.2020.07.061](https://doi.org/10.1016/j.neucom.2020.07.061).

Zhao, G., Sánchez-Azofeifa, G., Laakso, K., Sun, C., Fei, L., 2021. Hyperspectral and full-waveform lidar improve mapping of tropical dry forest's successional stages. *Remote Sensing* 13, 3830. doi:[10.3390/RS13193830](https://doi.org/10.3390/RS13193830).

Zolkos, S., Goetz, S., Dubayah, R., 2013. A meta-analysis of terrestrial aboveground biomass estimation using lidar remote sensing. *Remote Sensing of Environment* 128, 289–298. doi:[10.1016/j.rse.2012.10.017](https://doi.org/10.1016/j.rse.2012.10.017).

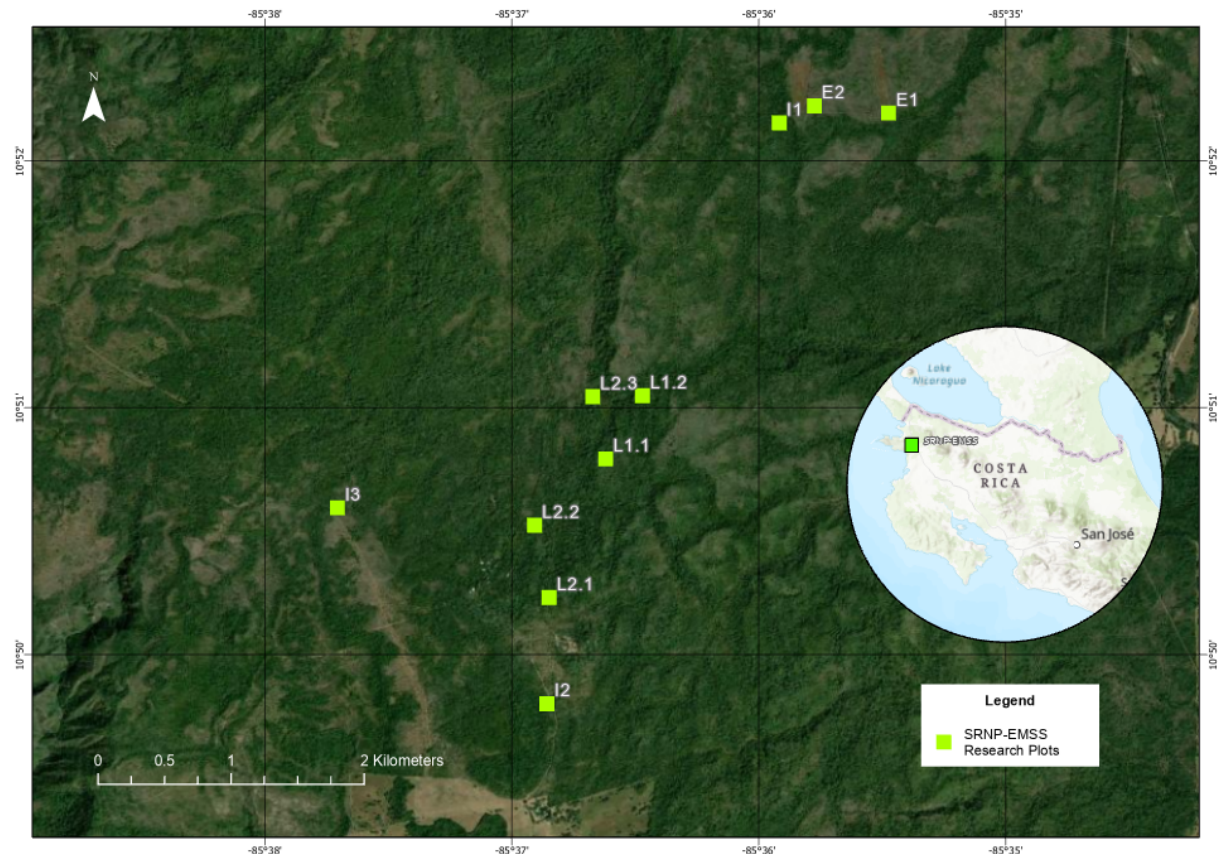


Figure 1: Locations of permanent research plots of the Santa Rosa National Park—Environmental Monitoring SuperSite (SRNP-EMSS). Ecological succession, measured as a function of time since abandonment, is divided into Early (E), Intermediate (I), and Late (L) forests. Source: Worldview-2 Satellite Image, Maxar Inc., 01/09/2019.

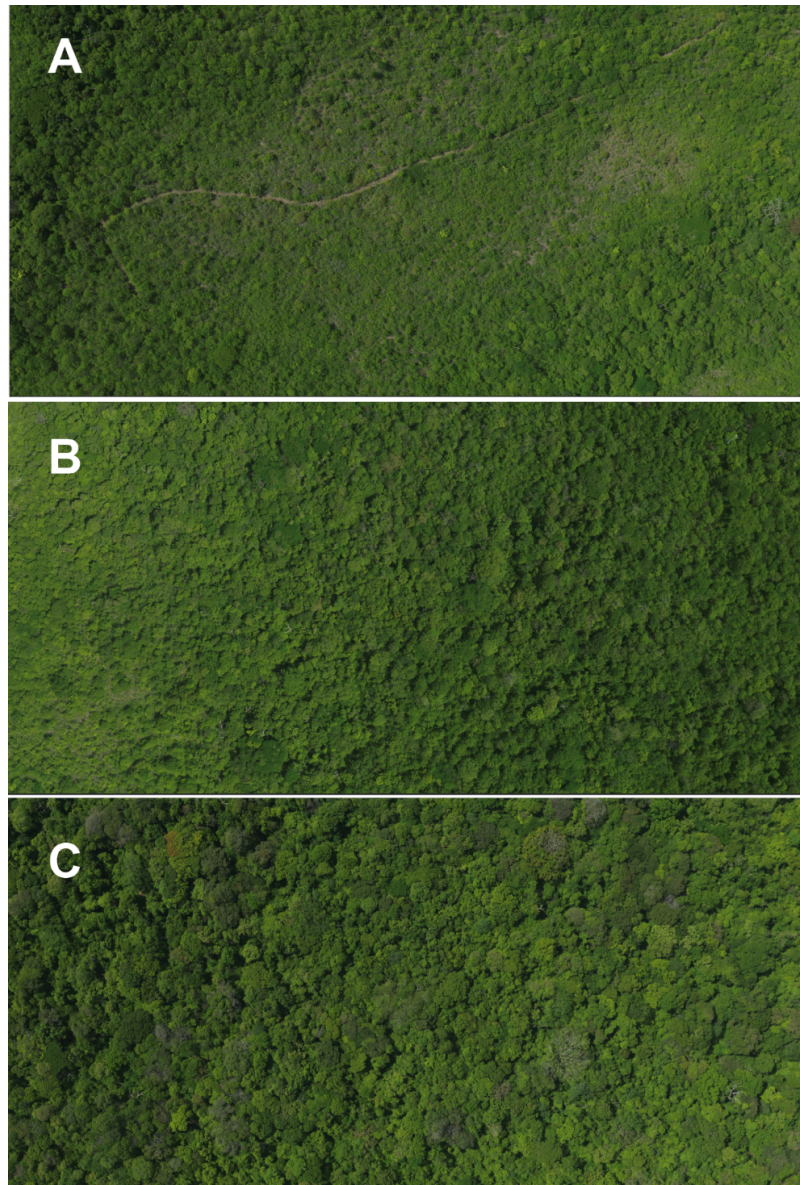


Figure 2: Aerial photographs capturing the SRNP-EMSS tropical dry forest canopy, illustrating (a) early stage, (b) intermediate-stage, and (c) late-stage tropical dry forest. All photographs were taken at the SRNP-EMSS in May 2021, using a Hasselblad H4D-50 aerial camera.



Figure 3: Comparison of point densities between the ULS_D (left) and ALS_D (right) laser scanning systems in plot E1. The ALS_D data exhibit a lower point density per square meter than the ULS_D data. ULS_D data were collected in March 2021, while ALS_D data were collected in May 2021.

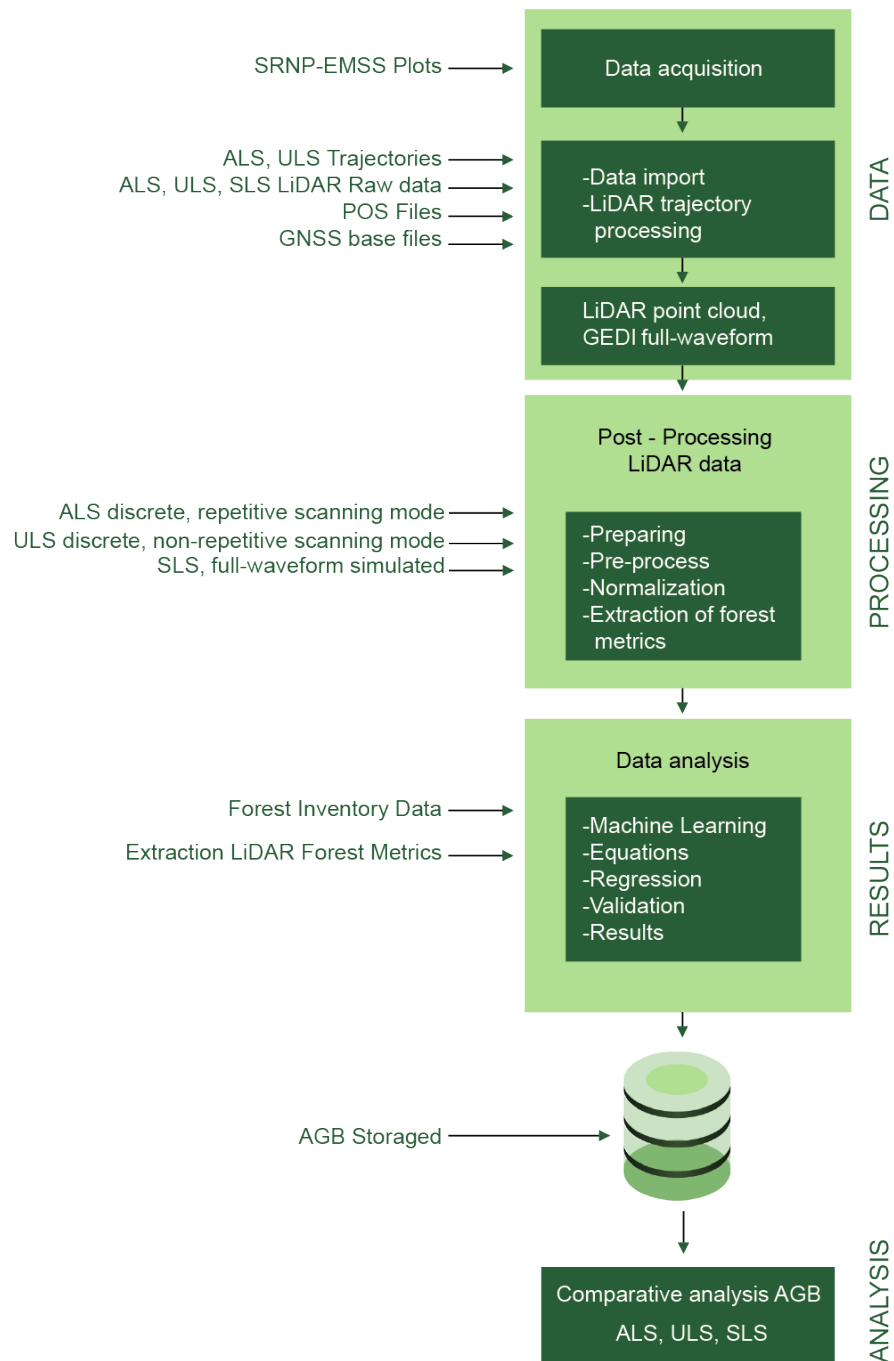


Figure 4: Workflow diagram illustrating the acquisition, post-processing, and analysis of LiDAR data from three laser scanning systems (ALS, ULS, and SLS) in the SRNP-EMSS plots. The process begins with data collection and georeferencing (data acquisition), followed by preparation, pre-processing, normalization, and extraction of forest metrics (post-processing). Then, forest inventory data are integrated, and various statistical and validation methods are used to estimate above-ground biomass (data analysis). Finally, a comparative analysis was conducted to assess the differences and advantages among the three systems (comparative analysis).

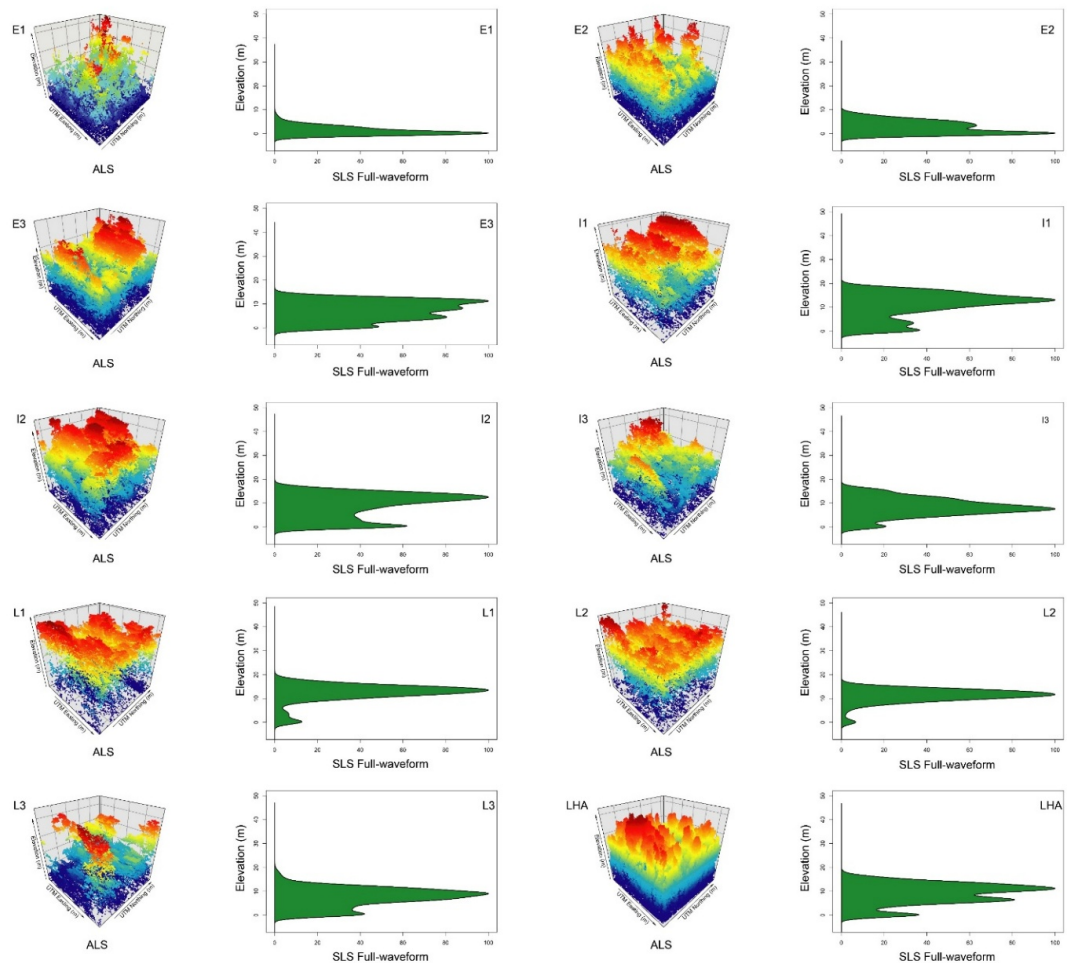


Figure 5: Three-dimensional point cloud representation of the ALS_D data and simulated SLS_{FW} signal derived from the ALS_D data for all plots.

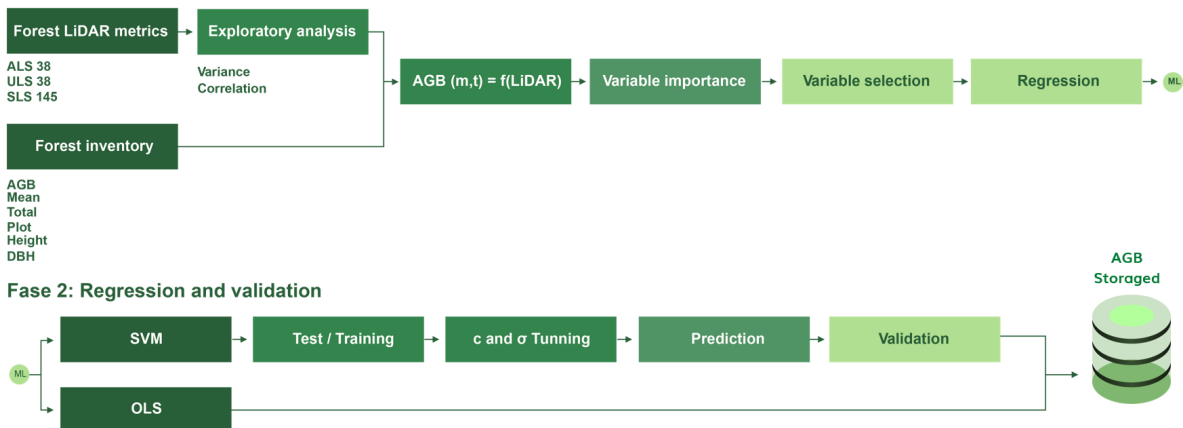
Phase 1: Data preparation

Figure 6: Schematic representation of the two-phase modeling workflow used to estimate Above Ground Biomass (AGB) from three laser scanning systems: ALS_D , ULS_D , and SLS_{FW} . In Phase 1 (Data Preparation), forestry LiDAR metrics were extracted and combined with field-derived forest inventory data (e.g., AGB, tree height, diameter at breast height), followed by exploratory analyses (variance, correlation) to determine suitable input features. In Phase 2 (Regression and Validation), Ordinary Least Squares (OLS) and Support Vector Machine (SVM) regression models were trained and fine-tuned (through hyperparameter optimization), and then validated using cross-validation. The resulting AGB estimates and their associated carbon storage metrics enable a comparative assessment of the performance of each laser scanning system.

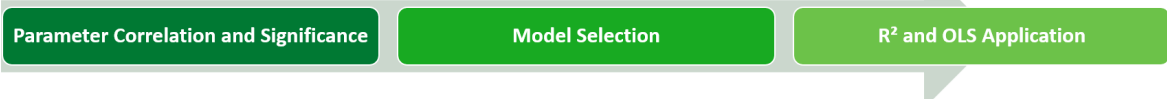
Laser Scanning Metric Selection**Regression Variable Selection**

Figure 7: Workflow for Laser Scanning Metric and Regression Variable Selection. The figure outlines a two-stage process for selecting metrics and variables for modeling above-ground biomass (AGB). The first stage focuses on laser scanning metrics, where initial checks eliminate metrics with zero variance, ensuring that only informative variables remain. Correlation analysis was then conducted, prioritizing metrics with a Pearson's correlation coefficient (ρ) below 0.5, which better represented independent contributions to AGB variability. Metrics were further filtered based on relative importance scores (≥ 0.5), and the three most critical metrics were selected when thresholds were not met. In the second stage, the regression variables are evaluated based on their correlation and parameter significance. Model selection emphasizes minimizing errors while maximizing the coefficient of determination (R^2), which quantifies the model's explanatory power. The workflow ensures robust, statistically sound modeling of the AGB using relevant and non-redundant variables.

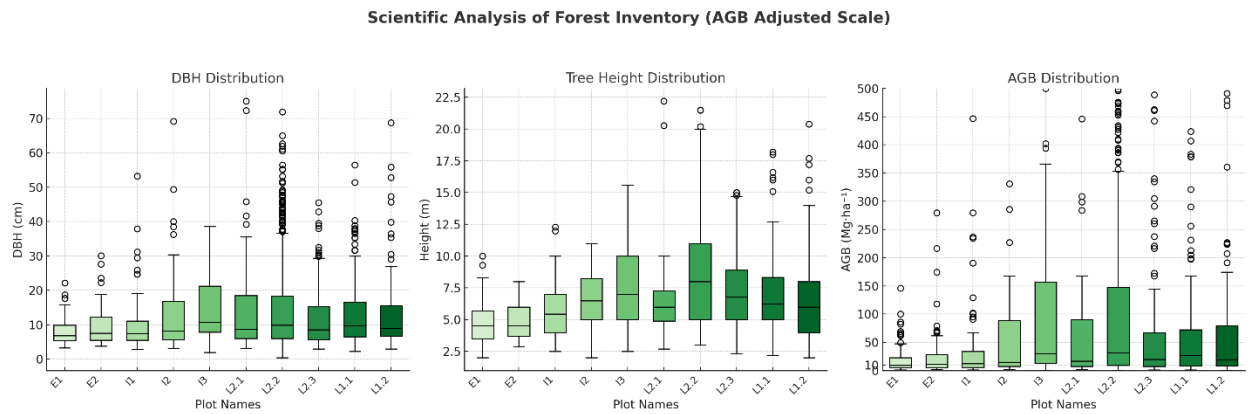


Figure 8: Box plots of the variables (a) DBH, (b) Height, and (c) *AGB* for the study plots at the SRNP-EMSS. Notations are as follows: E: early succession, I: intermediate succession, L: late succession.

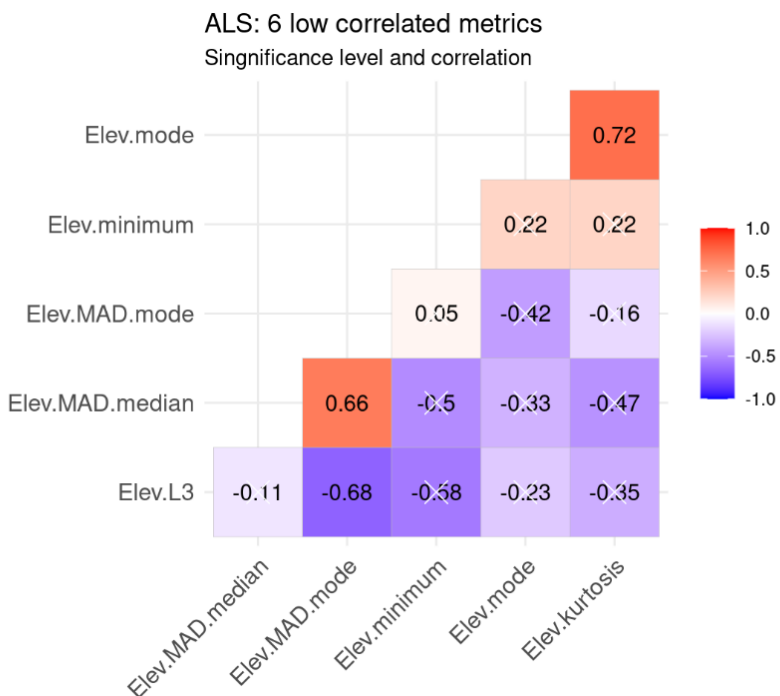
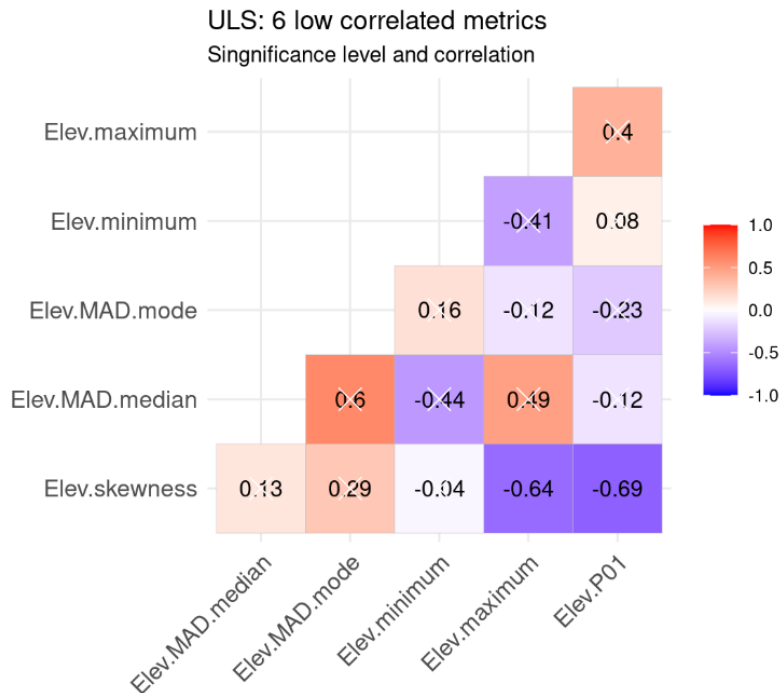
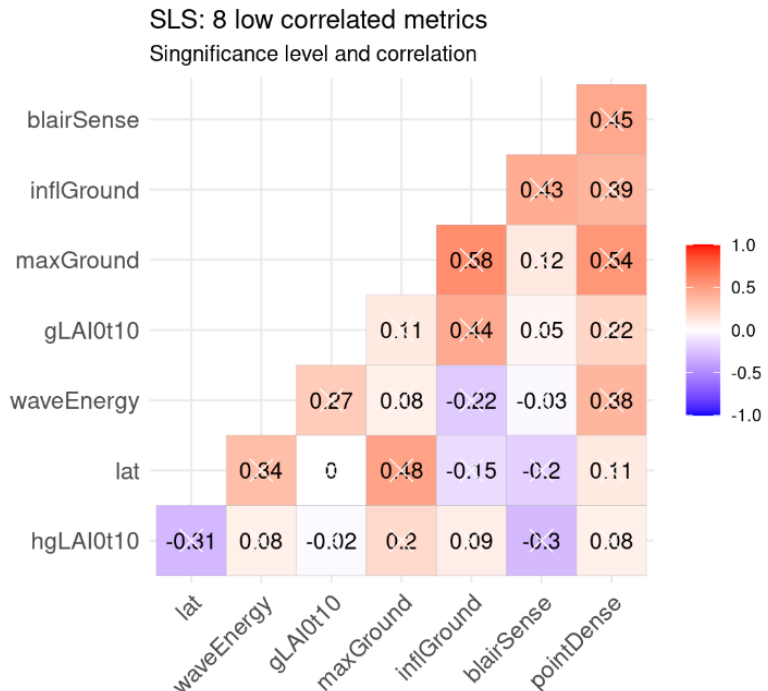


Figure 9: Correlogram of variables obtained from ALS_D .

Figure 10: Correlogram of variables obtained from ULS_D .Figure 11: Correlogram of variables obtained from SLS_{FW} .

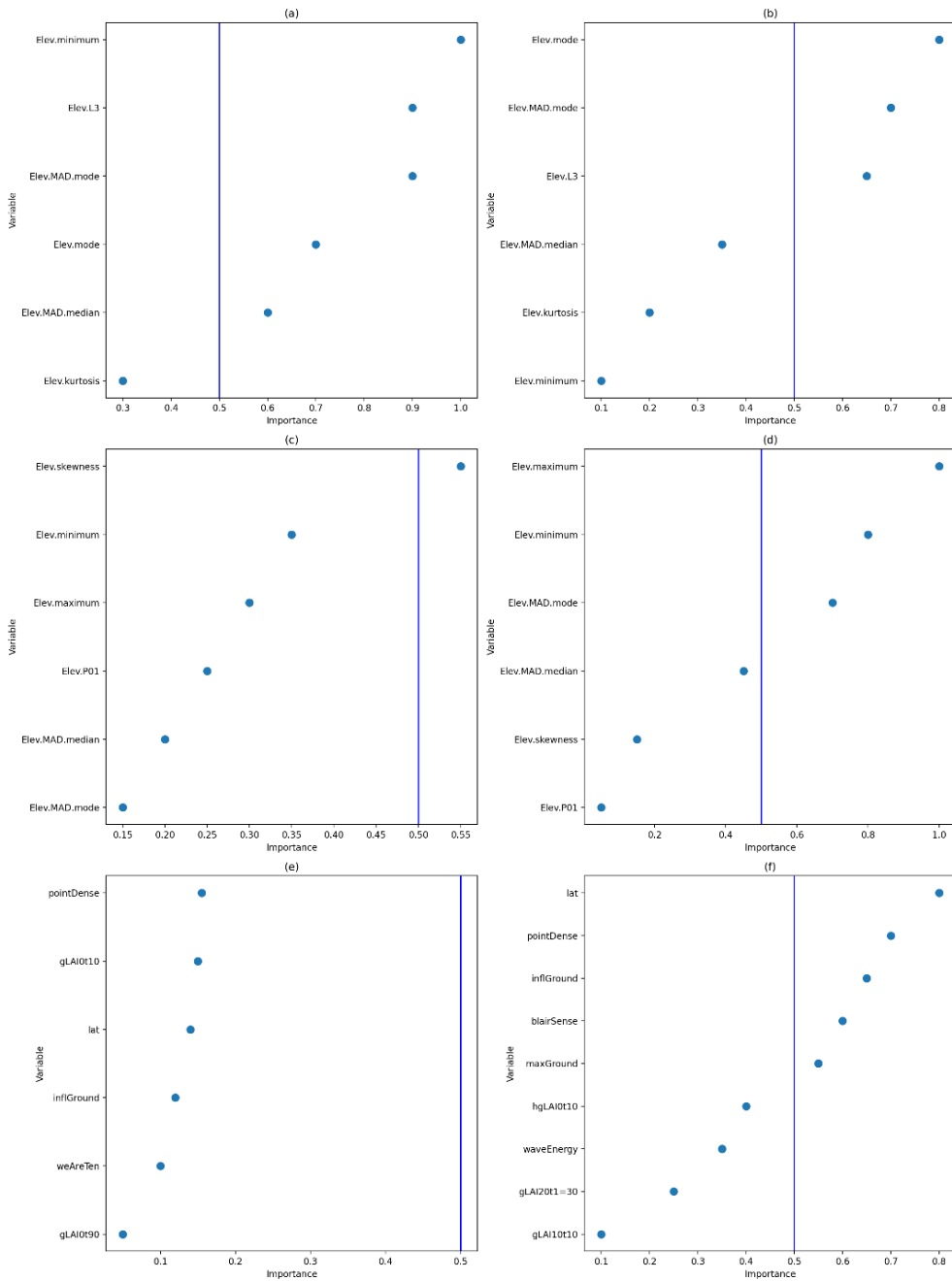


Figure 12: Relative importance of the ALS_i , ULS_i , and SLS_{FW} variables. (a) Relative importance of variables for modeling AGB_i with ALS_i systems. (b) Relative importance of variables for modeling AGB_m with ALS_i systems. (c) Relative importance of variables for modeling AGB_i with ULS_i systems. (d) Relative importance of variables for modeling AGB_m with ULS_i systems. (e) Relative importance of variables for modeling AGB_i with SLS_{FW} systems. (f) Relative importance of variables for modeling AGB_m with SLS_{FW} systems.

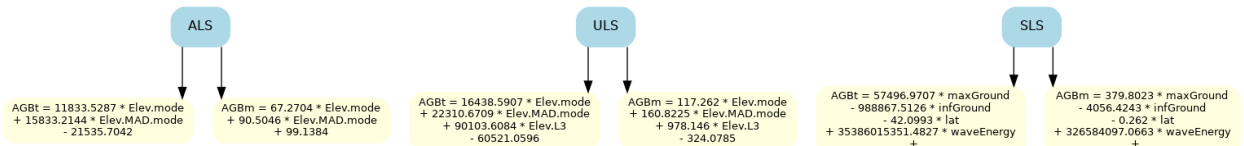


Figure 13: [Escribe aquí la descripción de la figura]

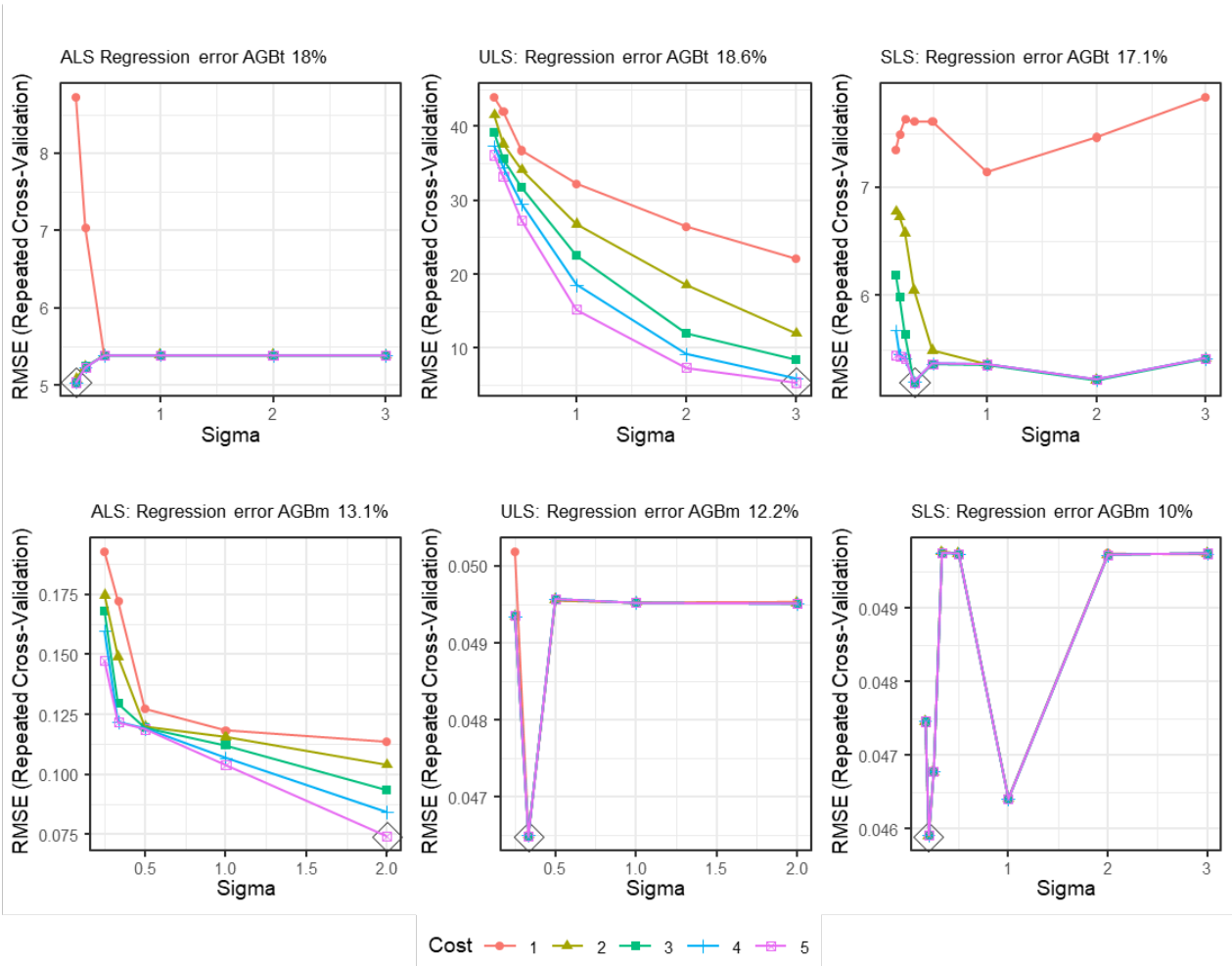


Figure 14: These six plots illustrate the optimization of hyperparameters during the estimation of AGB using SVM. The optimization was performed using a grid search method, where combinations of hyperparameters, such as sigma (kernel parameter) and cost, were systematically tested to minimize the estimation error. The plots show the progression of the Root Mean Square Error (RMSE) during repeated cross-validation for three different LiDAR platforms (ALS, ULS, and SLS) and two biomass estimation metrics (AGBt and AGBm). Each plot includes the following components: X-axis (Sigma): represents the kernel parameter, which controls the shape of the decision boundary in the SVM model. A lower sigma value leads to more flexible boundaries (complex models), whereas a higher sigma value results in smoother boundaries (simpler models). Y-axis (RMSE): Displays the RMSE during repeated cross-validation, which measures the model's prediction error. Lower RMSE values indicate better model performance. Lines (Cost): Different lines correspond to varying cost values, a regularization parameter that controls the trade-off between achieving a low error in the training data and minimizing the model complexity.

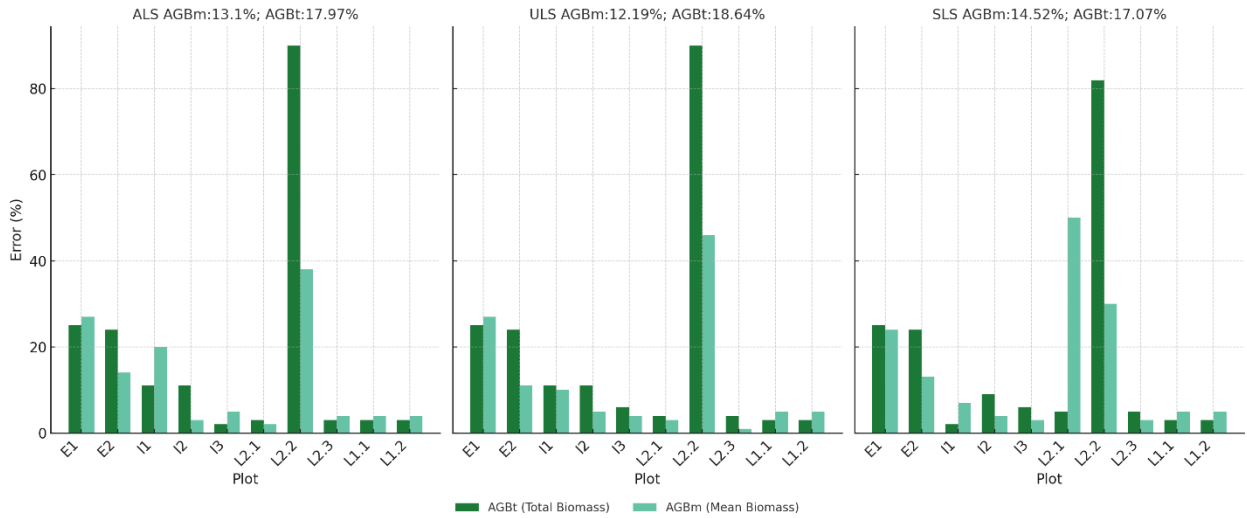


Figure 15: Percentage errors identified in the regression of AGBt and AGBm estimates using data from ALS_D , ULS_D , and SLS_{FW} .

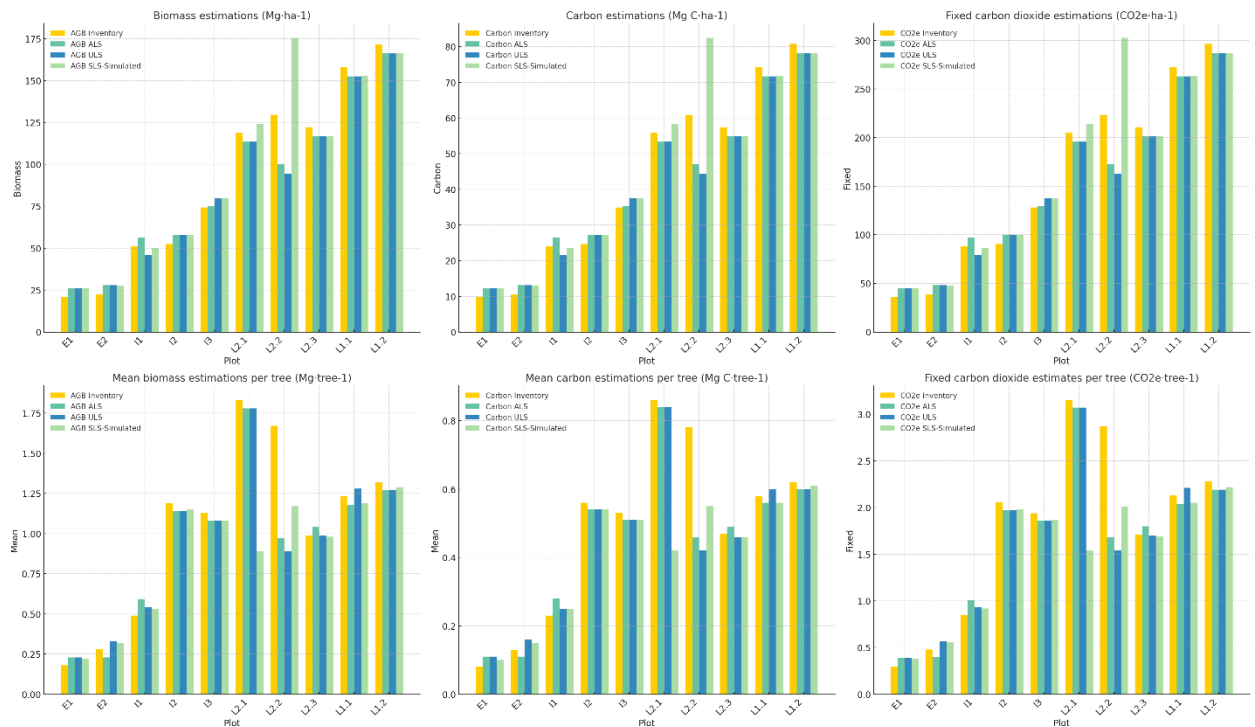


Figure 16: Results of the AGB estimates for Forest Inventory, ALS_D , ULS_D , and SLS_{FW} .

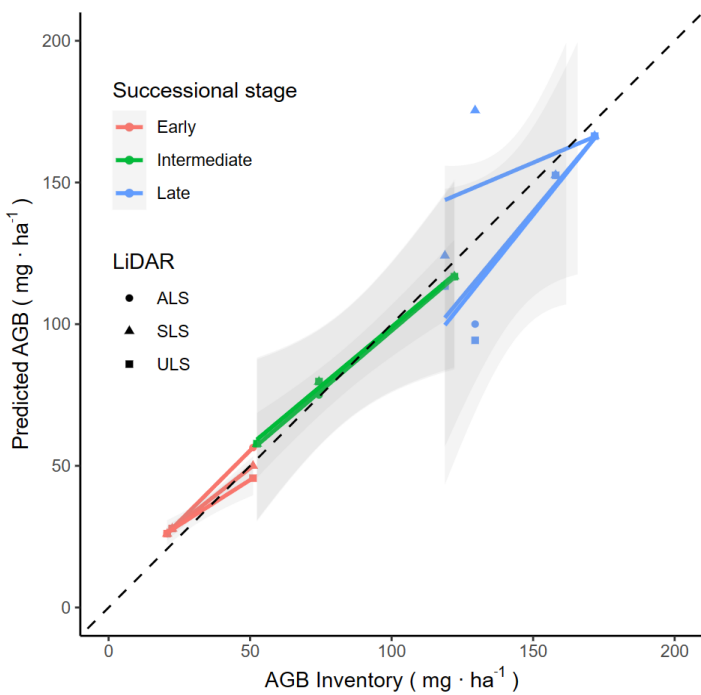


Figure 17: Results of the AGB estimates for ALS_D , ULS_D , and SLS_{FW} .